Modelling the Energy Yield of the PowerWindow

SHREEA SHARMA

Technische Universiteit Delft

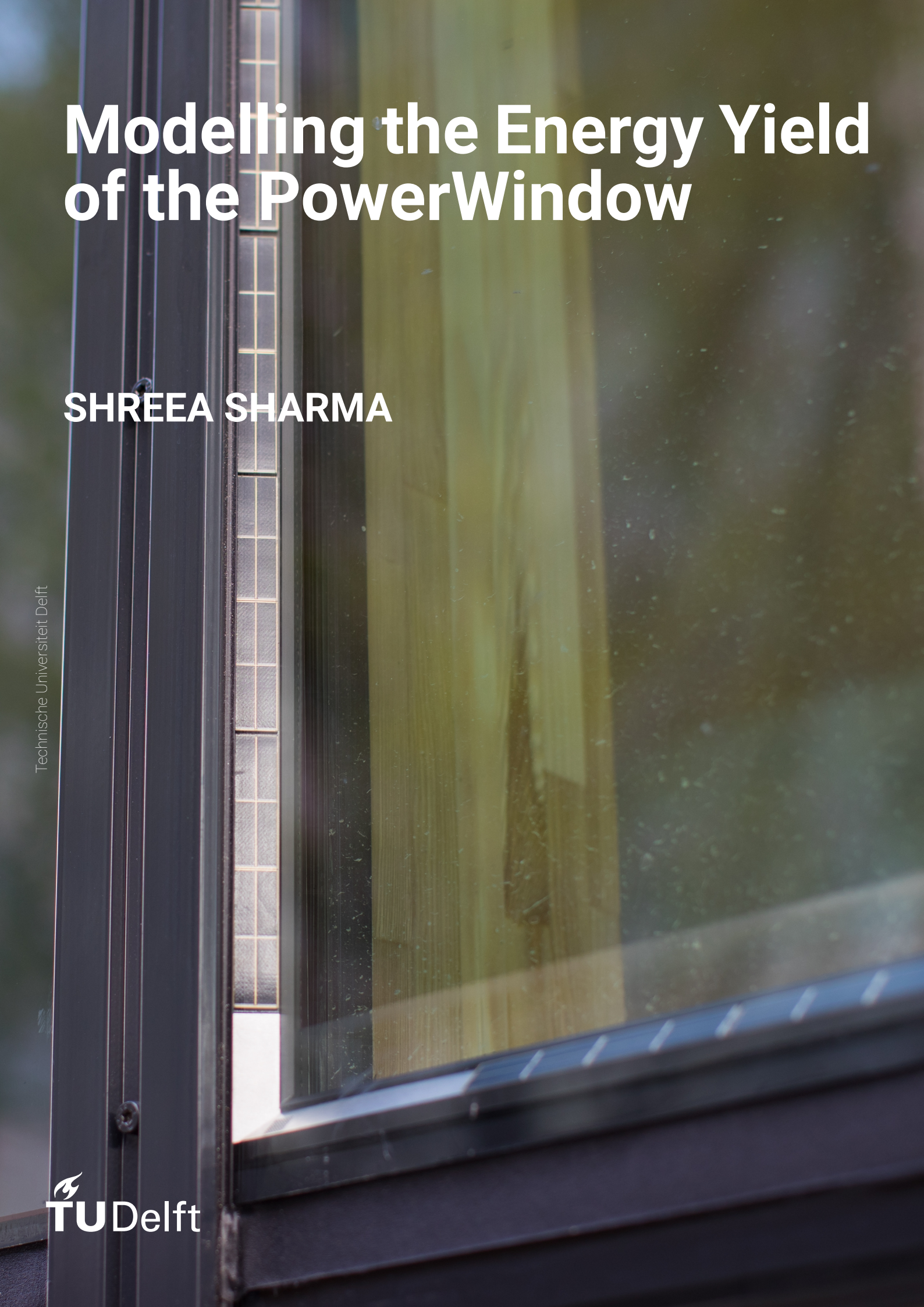

TU Delft

Modelling the Energy Yield of the PowerWindow

by

SHREEA SHARMA

In partial fulfilment of the requirements for the degree

MASTER of SCIENCE

in Microelectronics

29th March 2018

Student number:	4505093
Supervisor:	Prof. dr. A. A. H. M. Smets (TU Delft)
Daily Supervisors:	Dr. R. Santbergen (TU Delft)
	Mr. S. Anders (Physee)
Thesis Committee:	Dr. ir. R. v. Swaaij (TU Delft)
	Dr. ir. M. Ghaffarian Niasar(TU Delft)
	Mr. Pim Rutgers (Physee)

This thesis is confidential and cannot be made public until March 29, 2019.

TU Delft

PVMD Delft University of Technology

PHYSEE

Abstract

The European Union has established two directives that require both public and private buildings to become nearly zero energy by 2020. This has increased public interest in and development of building integrated photovoltiac (BIPV) systems. One such BIPV solution is the PowerWindow by Physee. Even though the PowerWindow does not produce as much power as a traditional rooftop installed photovoltaic solution, it can still be viewed as a step in the right direction to achieve sustainable development.

This thesis project aims at modelling the energy yield of the PowerWindow by developing a simple framework with optical, thermal and electrical models. This thesis also evaluates the electrical characteristics of the PowerWindow under solar simulators. Furthermore, opto-electronic parameter values like current, voltage, reflectance and so on found through experimentation are used as input to the models. The optical model deals with a ray tracing approach to find the incident irradiance on the solar cells inside the PowerWindow. This incident irradiance along with the weather data is used for the development of a thermal model to predict the temperature of the solar cells using a fluid dynamic approach. To model the electrical characteristics of the PowerWindow, a one diode equivalent circuit is used. However, the current source is modified to incorporate the effects of inhomogeneous irradiation on and the temperature of the solar cells.

The results of this work show that the maximum power produced by the PowerWindow, currently manufactured by Physee, is approximately 3.5 W under a solar simulator. This work also compares the incident irradiation profiles of all the edges of the PowerWindow, which produce power on different days, orientations and locations. The effects of shading on the PowerWindow is evaluated in terms of irradiation and is found to be present only in the summer months in Eindhoven. Furthermore, the daily energy yield calculated for a typical summer, winter and overcast day in Eindhoven is found to be 13, 5 and 3 Wh. It was concluded that a west and east facing PowerWindows in Eindhoven produce more energy in the summer and less in the winter as compared to a south facing PowerWindow. Additionally, the most performance effective circuit configuration is found to be the one with both blocking and bypass diodes.

Acknowledgement

I would like to express my sincere heartfelt gratitude to my daily supervisor Dr. Rudi Santbergen for supporting my work and providing me with feedback every step of the way. You've been a tremendous mentor and your patience is much appreciated. I would also like to thank Dr. Arno Smets (TU Delft) and Mr. Ferdinand Grapperhaus (Physee) for making this thesis possible. I would like to take this opportunity to acknowledge with much appreciation Mr. Sam Anders, my supervisor at Physee. Thank you for encouraging me and allowing me to grow at my own pace. I also thank the entire team at Physee for their support during my time at Physee.

A special thanks to Andres, Vimal and Matteo for continually helping me throughout my thesis. Words can not express how grateful I am to the three of you. Lastly, a big thank you to all my friends with whom I shared the last two and half years for making my life in the Netherlands fun by creating a great environment to live and study in. And also to my family for their utmost love and support.

SHREEA SHARMA
Delft, March 2018

Contents

List of Figures

List of Tables

1 Introduction

Our lives are set against the backdrop of climate change [1] and renewable resources are our best chance for fighting against it. This is because renewable sources (such as wind and solar energy) not only provide relatively low environmental impact while generating energy, but are also present abundantl, unlike traditional energy sources (such as fossil fuels) [2]. In the world, the most abundantly available energy source is sunlight. By utilizing on the order of 0.01% of the incident solar power we could satisfy humanity's yearly energy consumption [3]. Semiconductor devices such as solar cells can convert the energy coming from the sun into usable electrical energy via the photovoltaic effect. These devices can be fabricated using different materials and technologies, and are placed in a variety of geographical locations with varying irradiation levels [4].

In Europe, traditional buildings account for 40% of the energy consumption of and are responsible for more than a third of Green House Gas emissions. By the implementation of renewable system based technologies, new buildings can offer the greatest potential to reduce energy consumption by 30- 80 % [5, 6]. As a result, the European Union established two legislations including the *Energy Performance of Building Directive* which requires both public and private buildings to be nearly zero-energy buildings (NZEBs) by 2018 and 2020 respectively [7]. Consequently, clean energy solutions are needed in order to make the transition into sustainable development.

In a densely populated country like the Netherlands, the land use is allocated for agricultural, industrial and residential purposes. Especially in high-rise buildings, rooftop installed photovoltaic solutions may achieve the European directive; however there is a limited space available on the top of the buildings. Therefore, an architectural based solution needs to be implemented along with building applied photovoltaic systems such that the building envelope (facade) is able to produce the the required energy to make NZEBs. Building Integrated Photovoltaic (BIPV) systems provide this solution by replacing traditional building materials with photovoltaic material and technologies. One such BIPV technology is the *PowerWindow* by Physee. This device uses small area solar modules around the edges of a multi-glazed window. The concept of the PowerWindow is a step in the right direction in order to achieve the directives mentioned above.

1.1. PowerWindow by Physee

A PowerWindow is a fully transparent, electricity generating multi-pane window by Physee. It imparts an ordinary window with an extra functionality of generating power using solar energy.

In order to understand the layout of the PowerWindow (PW), the structure of an ordinary window needs to be established. An ordinary window consists of two or more glass panes that are held together by a spacerframe that provides a fixed offset between the glass panes. The spacerframe is made up of four aluminium beams running along the edges and connected at corners of the window by corner keys. Two of these beams are filled with moisture absorbing balls in order to prevent the window from fogging. The window panes and the spacerframe are glued together and sealed.

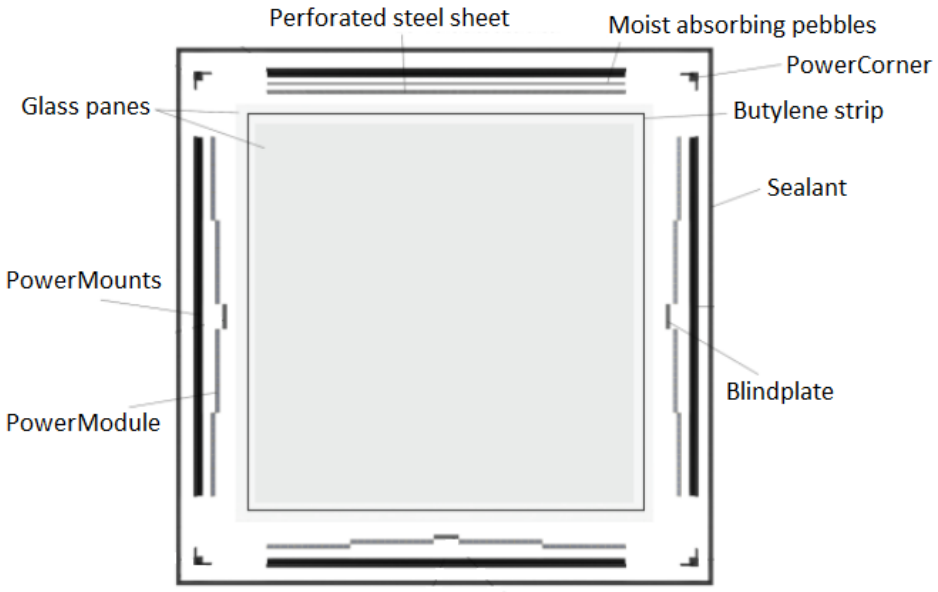

Figure 1.1: Layout of and components inside a PowerWindow.

In the case of the PowerWindow (see Figure 1.1), the difference in the layout lies in the spacerframe. It consists of four PowerMounts that are made of aluminium but instead of being flat, they are angled at 45 degrees as seen in Figure 1.2. This is done for two reasons:

1. to add functionality of hosting the photovoltaic cells mounted on a printed circuit board (PCB) - these are called PowerModules;

2. to ensure maximum amount of solar irradiation on the photovoltaic cells given the design constraints posed by the PowerWindow.

Out of the four PowerMounts, three of them are equipped with PowerModules. However, the last one is filled with the moisture absorbing balls that are kept in place with the help of a perforated steel sheet. Depending on the horizontal length of the window, a Blindplate (a plane aluminium sheet that is inserted in the PowerBar that fills up the leftover space) may be inserted next to the PowerModules to cover the empty space. The electricity generated is transported out of the window using cables.

1.1.1. Solar Components Inside a PowerWindow

The PowerWindow consists of Original Equipment Manufacturer (OEM) customizable solar cells and modules components by IXYS [8]. Physee uses back-contacted mono-crystalline solar cells. These monocrystalline silicon based solar technology has one of the highest efficiencies as compared to other solar cell technologies [4, 9]. Figure 1.3 shows the different solar components that make up the PowerWindow. A Solar cell KXOB22-12X1F cell by IXYS is the smallest OEM solar unit produced. The series connection of eight of these cells results in SLMD121H08L type C mini-module. Although Physee can tune the voltage between 8 - 24 V, it has standardised the voltage requirement to 12 V. This is because the PowerWindow is connected to a battery system that is used to store the power from the PowerWindow, and it requires 12 V to operate. The voltage is set by series connecting three mini-modules to make one PowerModule (PM). A PowerBar (PB) is made up of parallel connected PowerModules. The length of the PowerBar determines the current it produces. Since the PowerWindow dimensions often vary from building to building, the current of the PowerBar is not fixed, unlike the voltage. A PowerWindow contains only three PowerBars; one on the left, the right and the bottom side of the window. These PowerBars can be connected in series (to increase the final voltage) or parallel (to increase final current) depending on the requirements of the project. Table 1.1 displays the dimensions of all the solar components of the PowerWindow. It also contains a small summary of these components.

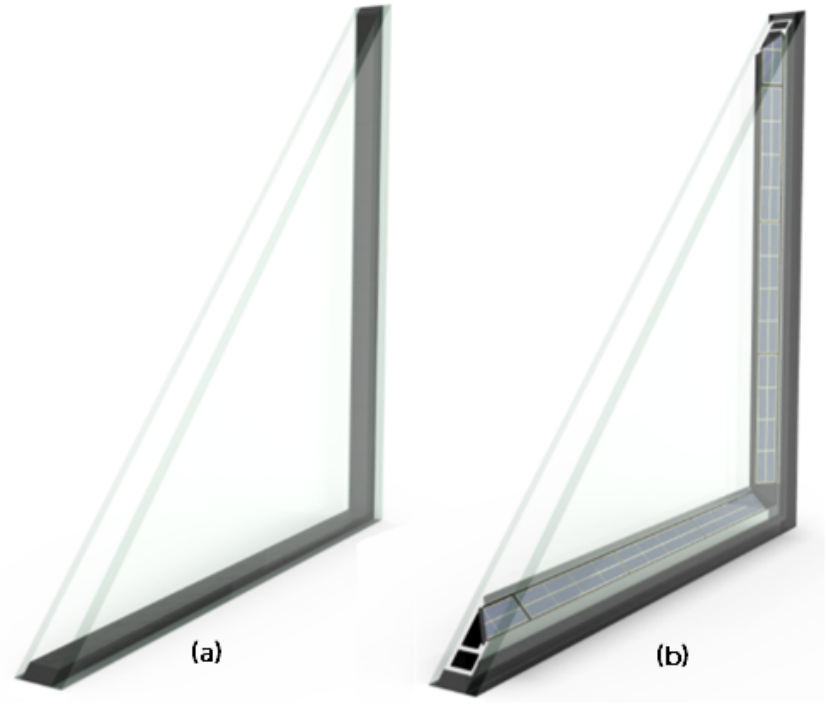

Figure 1.2: (a) Aluminium spacer beam in an ordinary window, (b) PowerMount with PowerModules in a PowerWindow by Physee.

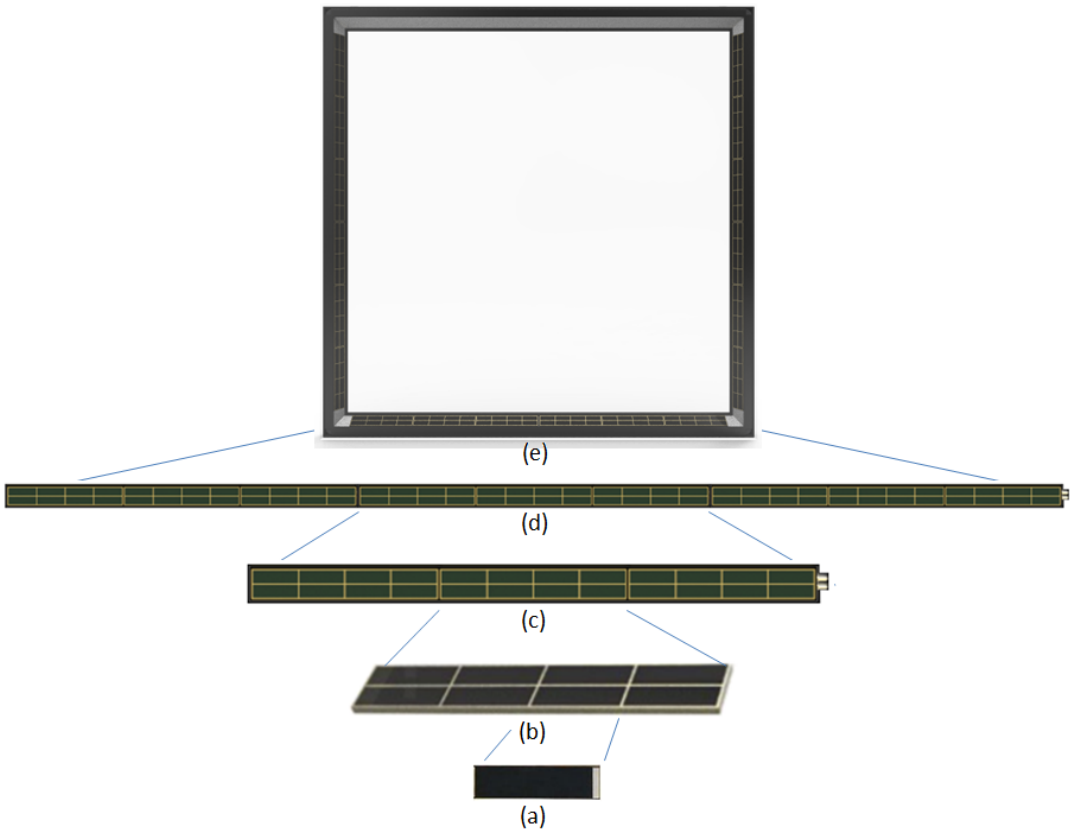

Figure 1.3: (a) Solar cell KXOB22-12X1F by IXYS, (b) SLMD121H08L Type C mini-module by IXYS, (c) PowerModule by Physee, (d) PowerBar with 3 PowerModules in parallel and (e) PowerWindow with 3 PowerBars in parallel.

Table 1.1: Dimensions of the solar components inside the PowerWindow.

Solar Component	**Dimensions** (mm) L×B×H	**Active Area** (mm^2)	**Brand**	**Notes**
Solar cell (KXOB22-12X1F)	22×7×1.8	154	IXYS Korea	Smallest solar product by IXYS
Type C mini-module (SLMD121H08L)	86×14×2	1204	IXYS Korea	Series connection of 8 KXOB22-12X1F cells
PowerModule (PM)	267×16×3	3612	Physee	Series connection of 3 SLMD121H08L mini-modules
PowerBar (PB)	-×16×3	-×PM	Physee	Parallel connection PMs depending on the length requirements of client
PowerWindow (PW)	-	3×PB	Physee	The dimensions depend on the requirements of the client. Can consist of either series or parallel connected PBs

1.2. Energy Yield Prediction

The energy yield of any photovoltaic (PV) system can be calculated provided there are certain input parameters available. The two crucial input parameters are irradiance incident on the PV modules and the corresponding temperature of these modules. With the help of these parameters, the final energy yield of the PV system can be estimated. Moreover, it is important to note that the incident irradiance on the module is needed to determine the temperature of the module. Figure 1.4 shows this process of using three different models is generally used to predict the energy yield of PV systems. For conventional rooftop PV systems there is commercial software for energy yield prediction available [10, 11]. However, for the more complex geometry of a PowerWindow, the conventional optical, thermal and electrical models cannot be used and dedicated models need to be developed.

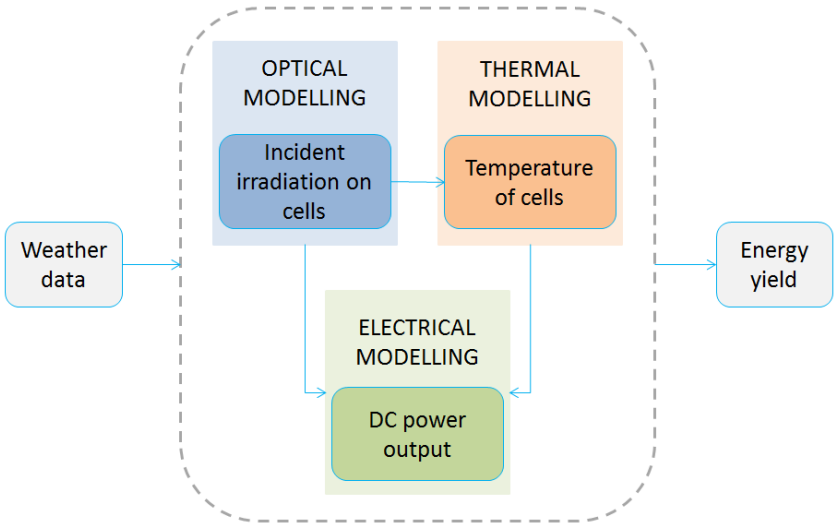

Figure 1.4: Development of framework in order to calculate the energy yield of the PowerWindow

1.3. Motivation for Thesis

The aim of a PowerWindow is to merge the power production capability of ordinary window with minimal alterations to the aesthetics and its underlining functionality of separating the outdoor climate from the indoor climate. Therefore, the PowerWindow by Physee is the first of its kind that offers a combination of both the above mentioned functionalities in ordinary window. As a result, there is a need to accurately predict the

energy yield this technology. Although, several optical [12–16], thermal [17, 18] and electrical models [19–22] have been developed for non-standard PV systems, none of these approaches have been used to estimate the performance of the PowerWindow and fully characterise its behaviour optically, thermally and electrically.

This thesis aims to address three different questions. These are listed as follows:

1. **What are the optical, electrical and opto-electronic characteristics of the PowerWindow?**
2. **How does the layout of the PowerWindow affect its DC output?**
3. **Does self-shading play an important role on the PowerWindow's DC output?**
4. **How do the blocking and bypass diodes affect the PowerWindow's DC output?**
5. **What is the energy yield of the PowerWindow in different orientations and climatic conditions?**

1.4. Outline of Thesis

Chapter 2 starts by explaining the need to conduct opto-electronic tests on the solar components inside the PowerWindow. It aims to characterise the PowerWindow through different opto-electronic experiments and use values obtained in the next chapters. The details of the optical model for simulating the incident irradiation is outlined and explained in Chapter 3. Chapter 4 explains the methodology for obtaining the temperature of the solar cells using a thermal model. Chapter 5 consists of the electrical model of the PowerWindow that evaluates its DC power output and daily energy yield for different situations. It uses the incident irradiance on and the temperature of the solar cells inside the PowerWindow obtained from chapter 3 and 4. Chapter 6 concludes by summarising the results obtained from all the chapters in the thesis and giving recommendations for future work.

2

Opto-Electronic Experiments

In order to predict the energy yield of the PowerWindow (PW), it is not only critical to analyse the behaviour of the solar components inside but also the glass used to make the PowerWindow. This experimental analysis will provide the input parameters for the models developed in the next chapters. To obtain the required input parameters, an experimental approach is used that starts from the smallest solar unit (solar cell) to the largest (PowerWindow), and compares them to their respective datasheets. This approach is called the '*bottom-up*' testing method. There is a need to experimentally check the values to the *theoretical* or datasheet values because of the fact that IXYS tests their cells at wafer level instead of cell or module level. The aim of chapter is to:

1. report the differences in the observed electrical values of the solar cells and modules to the ones claimed in the datasheet;
2. understand the electrical behaviour of the PowerWindow under solar simulators;
3. determine the optical, opto-electronic and electrical parameters values needed as input in the Optical (chapter 3) and electrical (chapter 5) chapters to further characterise the PowerWindow.

2.1. Characterisation Methods

An overview of the characterisation methods is given in Figure 2.1. In this section each of the methods is explained in more detail.

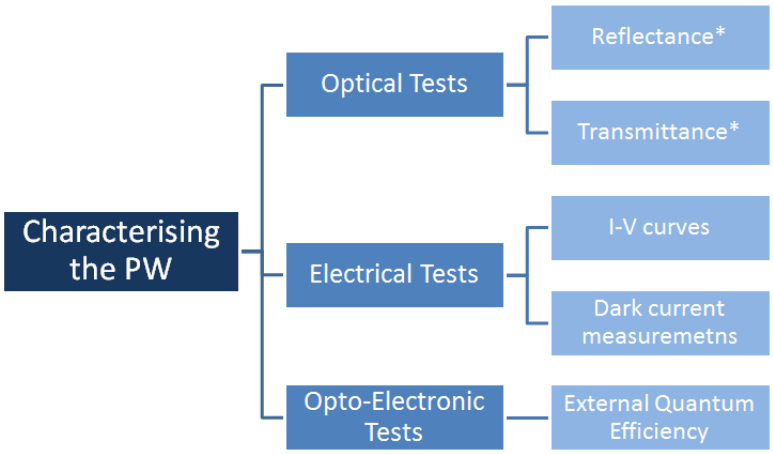

Figure 2.1: The different tests needed to fully characterise the PowerWindow, where * indicates tests required for glass.

2.1.1. Optical Testing

Reflectance and Transmittance

It is crucial to study the reflection properties of the mini-module by IXYS. This is because it gives information about the mini-module's average reflectance which can be used as a parameter for the optical simulations in chapter 3.

Moreover, Physee uses three types of glasses to manufacture their PowerWindows. These are float glasses that are given the names clear, coated and stripped, for convenience. The clear glass, a type of float glass (soda-lime) that is flat, has a uniform thickness. The coated glass is made up of a clear glass with an anti-near-infrared (anti-NIR) coating to prevent the transmission of NIR light. When the coating on the clear glass is mechanically removed, it results in the formation of stripped glass. Therefore, the reflective properties of glass (that is used for making a PowerWindow) needs to be determined in order to estimate the amount of light that will be received by the cell after it passes through the glass.

Similarly, the transmission properties of glass (clear, coated and stripped) need to be studied in order to estimate its optical properties. This will aid in estimating the irradiance incident on the cells.

2.1.2. Electrical Testing

Current(I)-Voltage(V) and Power(P)-Voltage(V) Characteristics

The I-V and P-V relationship characteristics of a solar component determines the electrical behaviour of that particular component. This characterisation technique gives a comprehensive representation of the cell's ability to convert light to usable electricity. It also helps in defining the *operating point* of the cell at which the maximum power (P_{mpp}) can be obtained. This further enables us to keep the device performing under such an operating condition where the output of the device is maximised. The I-V and P-V measurements are not only performed at standard test conditions, but also as a function of irradiance on the cell and the temperature of the cell [23].

Temperature dependent I-V and P-V curves are vital to predict the loss in performance when operating under real-time conditions. Electrical parameters such as voltage, power and current depend on temperature. As temperature increases, the open circuit voltage reduces significantly while the current increases slightly. This results in a reduction of power and efficiency of the solar cell [4]. Therefore, performing such experiments can help us calculate the percentage by which these parameters are affected.

Conducting such experiments in outdoor conditions under actual sunlight at any point of the day is not a reliable method. This is because, the irradiance, ambient temperature and wind speed cannot be controlled in such a situation. Therefore, a more appropriate form of measurement technique of the illuminated I-V and P-V characteristic curves must involve the use of a solar simulator [24].

Dark Current Measurements

Dark I-V curves measurements are equally important as measuring the output of the solar cells in light conditions. They are meant for diagnostic purposes since they provide additional information about the diodes (solar cells). These measurements are used to provide information about the ideality factor of the solar cells [24, 25].

2.1.3. Opto-Electronics Testing

External Quantum Efficiency (EQE)

External Quantum Efficiency or EQE(λ) of solar cell is the ratio between the number of photons that are incident on the cell and the number of electron-hole pairs it successfully collects at the contacts, as a function of wavelength. It determines the current that will be produced by the cell when exposed to photons of wavelength λ [4].

The EQE obtained over the entire spectrum can be used evaluate the loss mechanisms like parasitic absorption in layers such as the transparent conductive oxide (TCO) layer, anti-reflection coating, the barrier protection coating (for example EVA), back contact, etc. This characterisation technique facilitates in determining whether the design of the solar cell is optically effective or not [4].

The equipment used at the Photovoltaic Materials and Devices (PVMD) group at TU Delft was built in-house. The photon flux of the light source and the EQE of the sample is measured by determining the EQE of the reference photo-diode under the same conditions including temperature conditions and light source (calibration). A *Xenon discharge lamp* is used as a light source since it has broad spectrum pertaining to the solar cell performance range.

The short-circuit current density (J_{SC}) is calculated using the following equation 2.1 [4].

$$J_{sc} = -q \int_{\lambda_1}^{\lambda_2} EQE(\lambda) \phi_{ph,\lambda}^{AM1.5} d\lambda \tag{2.1}$$

Where q is the elementary charge (= 1.60217662 × 10^{-19} coulombs), ϕ is the photon flux in $m^{-2}sec^{-1}$ and λ is the wavelength in nm.

2.1.4. Theoretical Electrical Parameters of the Solar Components

The values of the electrical parameters have been taken from the datasheets provided by the manufacturer of the solar cells [26] and mini-modules [27]. These values are called the '*theoretical values*' since they represent those reported by IXYS. Moreover, the values officially reported have been used to estimate the *theoretical values* of the electrical parameters of PowerModule, PowerBar and PowerWindow. Table 2.1 displays the electrical parameter values of the solar components inside the PowerWindow. These values are for a 1 m^2 PowerWindow and the effect of tilt angle and the glass have not yet been taken into consideration. The 1 m^2 window consists of 4 PowerModules connected in parallel to form a PowerBar and 3 PowerBars are connected in parallel to make the solar component of the PowerWindow.

Table 2.1: Theoretical electrical parameter values of the solar components inside and of the (1 m^2) PowerWindow at Standard Test Conditions.

Solar component	$\mathbf{V}_{oc}$ (V)	$\mathbf{I}_{sc}$ (mA)	$\mathbf{V}_{mpp}$ (V)	$\mathbf{I}_{mpp}$ (mA)	$\mathbf{P}_{mpp}$ (W)	**FF** (%)
Solar cell	0.63	50.0	0.5	44.6	0.02	> 70
Mini-module	5.04	50.0	4.0	44.6	0.178	> 70
PowerModule	15.12	50.0	12.0	44.6	0.535	> 70
PowerBar	15.12	200	12.0	178.4	2.14	> 70
PowerWindow	15.12	600	12.0	535.2	6.42	> 70

2.2. Optical Properties

2.2.1. Reflectance of Glass

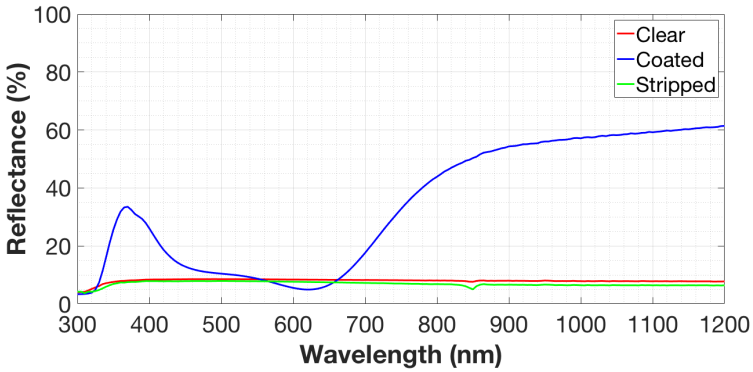

Figure 2.2: Reflectance profile of 3 different types of glasses.

The equipment used to measure the reflectance was the Perkin Elmer Lambda 950 UV/Vis spectrometer.The reflectance profiles for clear (red), coated (blue) and stripped (green) glasses are given in Figure 2.2.

It can be seen that reflectance profile for stripped and clear glass have a nearly wavelength independent reflectance of about 8 % throughout the wavelength range. The coated glass has a very different reflectance profile. It has a reflectance between 5 % and 30 % in the visible region (390 - 750 nm) and it reflects 45 - 60 % of light in the infrared region (> 800 nm). A reflectance peak is seen around ≈ 370 nm.

It should be noted that for the optical simulations, the average reflectance value of the stripped glass in the wavelength range of 300 - 1107 nm will be used. This is because the bandgap of mono-crystalline silicon is 1.12 eV and it corresponds to a wavelength of 1107 nm. Therefore, the solar cell will absorb all wavelengths less than 1107 nm. The average reflectance of all three glasses for the 300 - 1107 nm wavelength range is given in Table 2.2.

Table 2.2: Average reflectance of clear, coated and stripped glass over the 300 - 1107 nm wavelength range

Glass type	Average Reflectance (%)
Clear	8
Coated	31
Stripped	7

2.2.2. Reflectance of Mini-Module

In order to determine the average reflectance of a mini-module, it was necessary to perform its reflectance measurements over the 300 - 1200 nm wavelength range (Figure 2.3). The average reflectance was determined for the wavelength range 300 -1107 and was found out to be ≈ 5 %.

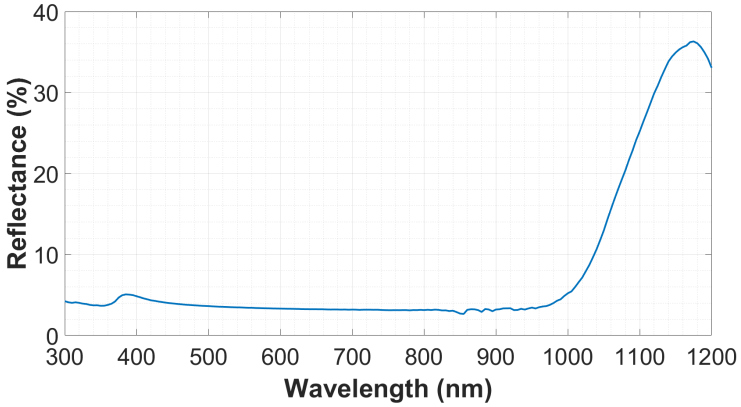

Figure 2.3: Transmission profile of a mini-module.

2.2.3. Transmittance of Glass

The same equipment to measure the reflectance was used. While the clear and stripped glass have relatively similar transmission profiles, the coated glass has a very different profile than the other two (Figure 2.4). Since the coated glass is used to prevent the transmission of near-infrared (NIR) light through it, the transmittance of the coated glass reduces from ≈ 15 % at 800 nm to almost 0 % at 1200 nm. As a result of the mechanical stripping of the anti-NIR coating from clear glass, the stripped glass has scratches that reduce its transparency somewhat compared to the clear glass. Therefore, the transmittance of stripped glass is less than that of clear glass. Similar to Table 2.2, the average transmittance of clear, coated and stripped glass over the 300 - 1107 nm wavelength range is listed in Table 2.3.

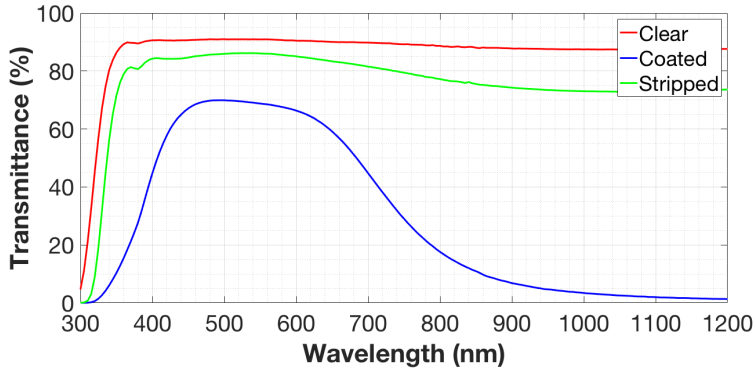

Figure 2.4: Transmission profile of 3 different types of glasses.

Table 2.3: Average transmittance of clear, coated and stripped glass over the 300 - 1107 nm wavelength range

Glass type	Average Transmittance (%)
Clear	87
Coated	31
Stripped	77

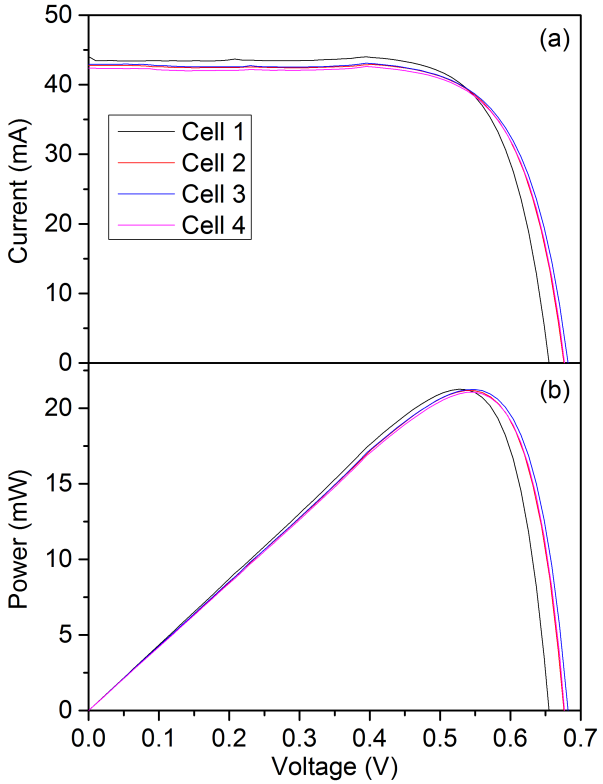

Figure 2.5: (a) I-V curves and (b) P-V curves for four randomly selected solar cells at Standard Test Conditions.

2.3. Solar Cell

2.3.1. IV and PV Characteristics

The solar cell measurements were first performed at Standard Test Conditions (AM1.5, 1000 W/m^2 at 25 °C) using a solar simulator by WACOM and 2601B SYSTEM SourceMeter by Keithley. In order to observe the typical performance of a solar cell, 4 cells were selected at random and their I-V (Figure 2.5 (a)) and P-V curves (Figure 2.5 (b)) were plotted.

As it can be seen from 2.5, three of the solar cells (cell 2, 3 and 4) have almost the same I-V and P-V curves. However, cell 1 has a slightly larger current value and smaller voltage value as compared to its counterparts. The measured electrical parameter values and their relative error are presented in Table 2.4. As observed from Table 2.4, the electrical parameter values have a relative error of ≤ 2 %, with a relative error of < 0.5 % for power. Compared to the rated values given in the datasheet, the I_{sc} and I_{mpp} values are ≈ 13 to 15 % lower than the rated values. While V_{oc} and V_{mpp} values are ≈ 6 to 8 % higher. The deviation in power is about 5 %.

Table 2.4: Values of the measured electrical parameters and their relative error of the solar cells by IXYS.

Parameters	Value	Units
V_{oc}	0.67 ± 2 %	V
I_{sc}	43.0 ± 1 %	mA
V_{mpp}	0.54 ± 2 %	V
I_{mpp}	39.0 ± 2 %	mA
P_{mpp}	21.15 ± 0.4 %	mW

2.3.2. EQE

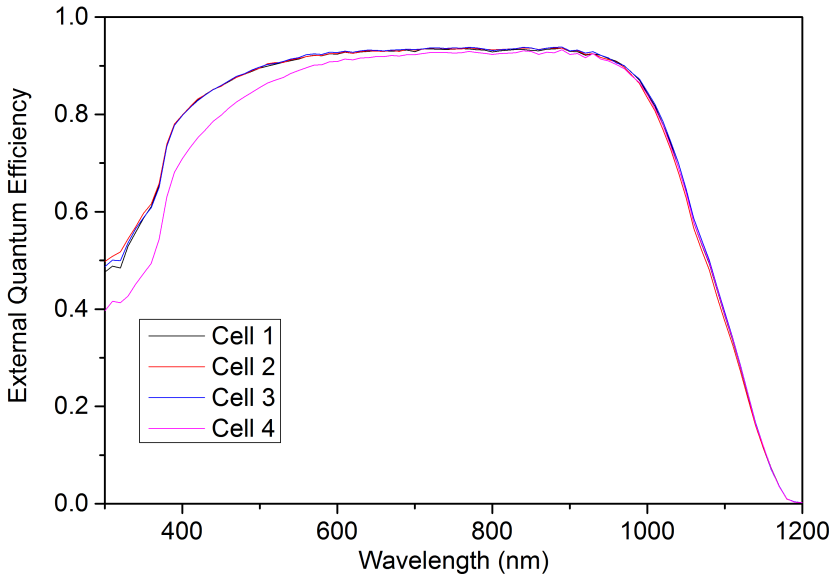

Figure 2.6: EQE curves for four randomly selected solar cell at Standard Test Conditions (STC).

The same four (randomly) selected solar cells were characterised optically to measure their EQE. Figure 2.6 displays the EQE curves for these four solar cells. As we can see, the behaviour of the solar cells is almost similar. The EQE is lower in the short wavelength range as a result of recombination at the front surface of the solar cell. The anti-reflection coating present at the front surface can be responsible for absorbing light in this range as well [4]. It is a relatively flat EQE line from the 600 to 900 nm range. This can be attributed to a homogeneous reduction of the overall quantum efficiency by the anti-reflection coating. The drop in EQE

beyond 1000 nm is due to reduced absorption of light in silicon at these larger wavelengths. Around 1180 nm, no light is absorbed since at those wavelength are below the bandgap of these solar cells. The mean measured value of the J_{sc} was found to be 38.16 mA/cm^2 with a relative error of < 1 %. Whereas, the difference between the mean measured value and the value in the datasheet is 11 %.

2.4. Mini-Module

2.4.1. I-V and P-V characteristics

The experiments were performed on one mini-module at PVMD under a solar simulator by WACOM. I-V and P-V curves were measured at 7 different temperatures ranging from 25 to 55 °C. Temperatures beyond 55 °C could not be reached due to the limitation of the equipment used. However, the temperature range and the number of readings noted are enough to evaluate the temperature coefficients of I_{sc} and V_{oc} of the mini-module.

Figure 2.7 (a) displays the temperature dependent behaviour of the I versus V of the mini-module. It can be observed that as the temperature increases, there is a reduction in the V_{oc} and a small rise in the I_{sc} of the mini-module. Since the decrease in the voltage is more than the rise in the current of the mini-module, the power produced by it must also decrease as a function of temperature. This is indeed seen in the Figure 2.7 (b). The thermal coefficients of I_{sc} and V_{oc} can be determined by plotting the measured I_{sc} and V_{oc} values individually against temperature as shown in Figure 2.7 (c) and (d). By establishing a trend line across these points, the slope of the line gives the thermal coefficient. In Figure 2.7 (c), the slope of the line is 0.02 mA/°C. Since current remains the same across each cell in series, the area of only one solar cell (1.54 cm^2) is used to arrive at the temperature in terms of current density. Thus, the thermal coefficient of J_{sc} was found to be 0.013 mA/cm^2°C. Similarly, the thermal coefficient of V_{oc} for the mini-module was found out to be -12.8 mV/°C. This is the value for series connected cells. The temperature coefficient for one cell, can be calculated by dividing this coefficient by the number of series connected cells, which in this case is 8. As a result, for one cell, the thermal coefficient of V_{oc} is -1.6 mV/°C. So the cell's voltage reduces by 1.6 mV per degree rise in temperature. Table 2.5 presents both the measured and rated thermal coefficients of I_{sc} and V_{oc}, as well as their percentage difference.

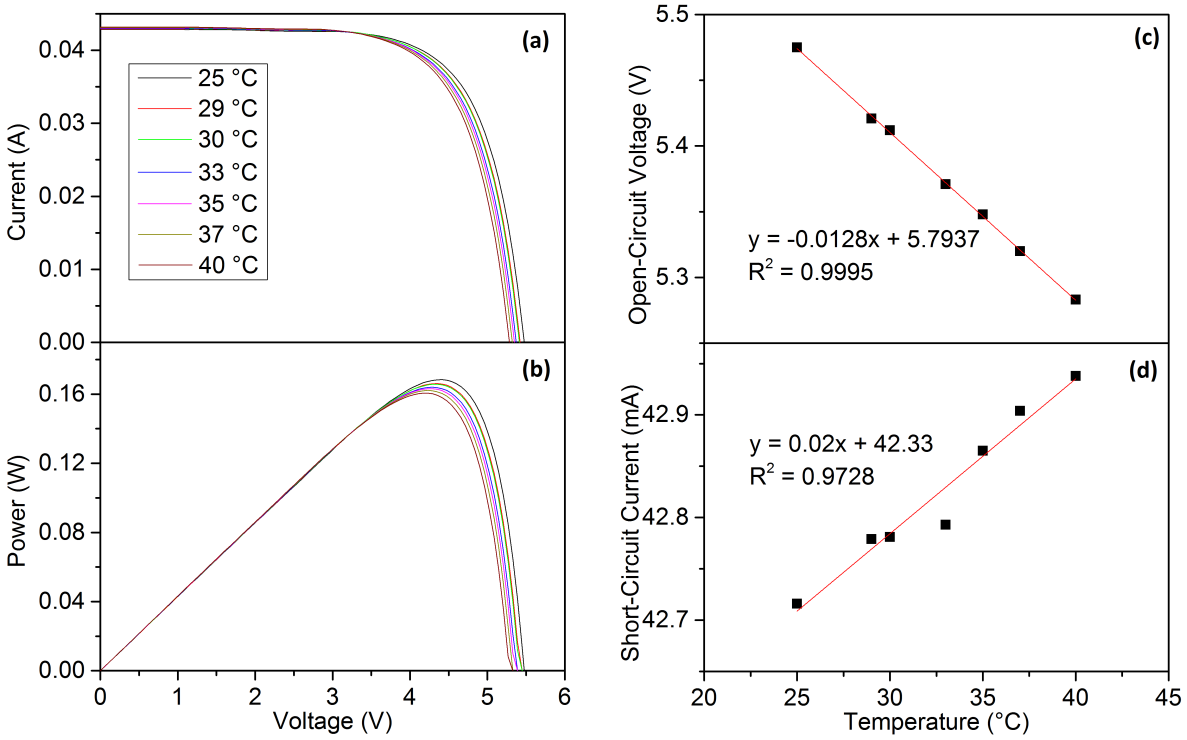

Figure 2.7: Temperature dependent (a) I-V, (b) P-V (c) V_{oc} versus temperature and (d) I_{sc} versus temperature curves for a mini-module at 1000 W/m^2.

Table 2.5: Measured and datasheet (rated) values of thermal coefficients of electrical parameters for a solar cell.

Parameters	**Measured**	**Rated**	**Percentage difference** (%)
I_{sc} (mA/°C)	0.02	0.18	160
J_{sc} (mA/cm^2°C)	0.013	0.12	160
V_{oc} (mV/°C)	-1.6	-2.1	27

2.4.2. Dark Current Measurements

A Keithley 6517A electrometer was used to perform the experiments. The ideality factor (n) of the solar cell can be measured by plotting the dark I-V on a semi-logarithmic scale i.e. natural log of the current versus the voltage (see Figure 2.8). The n is determined by the slope of the curve between the voltage range 1 to 7 V [25]. The value of n for a mini-module was found out to be 10.31. Since 8 solar cells are connected in series to make a mini-module, the n for a solar cell is 10.31/8 which is equal to 1.28.

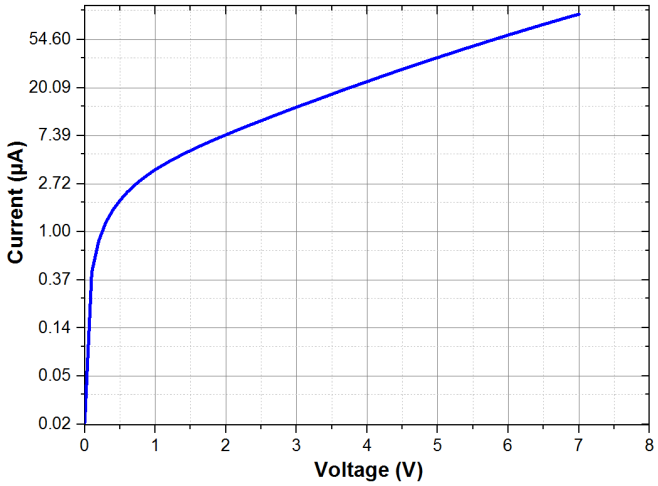

Figure 2.8: Dark forward I-V curve of a mini-module in a semi-logarithmic scale.

2.5. PowerModule

2.5.1. I-V and P-V Characteristics

The I-V curves for a PowerModule (PM) under different conditions need to be obtained in order to fully understand and predict its behaviour when placed at 45° and under stripped glass conditions. It is important to benchmark different conditions similar to the ones mentioned above. These conditions are presented in Table 2.6. The test set-up used in this experiment was the Large Area Solar Simulator (LASS) at PVMD, TU Delft. A temperature sensor was placed under the PowerModule, and the electrical as well as temperature data was recorded using a software that the LASS is connected to. As mentioned in the previous section, clear glass is glass that has no coating on it and has a transmittance of > 90 %. Coated glass has an anti-infrared coating on it that reflects most of the near infra-red and infra-red light, and some part of the visible light. The anti-IR coating is placed on top of the clear glass. The stripped glass is obtained when this anti-IR coating is removed from clear glass through a mechanical process.

Figure 2.9 graphically represents the above mentioned scenarios in terms of I-V measurements. The solid lines represent 0° tilt conditions while the dotted lines represent their 45° tilted counterparts. Clearly, the current produces by the PowerModule dramatically reduced when glass was placed in front of it. This effect was the highest for coated glass. A slightly different trend was noticed with the voltage. While the V_{oc} remains appreciably similar for scenarios 1, 2 and 3, it was lower for scenario 4. This is because of the reduction in the light generated current (I_L) produced was beyond 50 % and this affected the V_{oc} as they are related to each other by the equation 2.2.

Table 2.6: Different test case scenarios for one of PowerModule.

Scenario	Tilt Angle (°)	Glass	Glass type
S1	0	No	-
S2	0	Yes	Clear
S3	0	Yes	Coated anti-NIR
S4	0	Yes	Stripped anti-NIR
S6	45	No	-
S7	45	Yes	Clear
S8	45	Yes	Coated anti-NIR
S9	45	Yes	Stripped anti-NIR

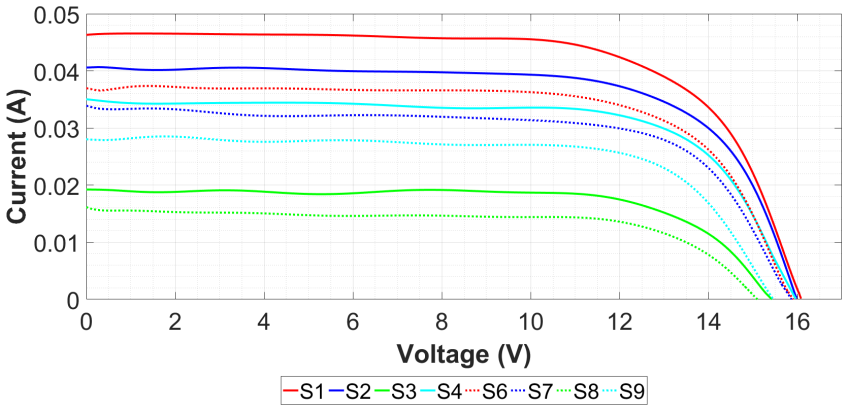

Figure 2.9: I-V curves for different test case scenarios for one PowerModule where 'Scenario' is abbreviated to 'S'.

$$V_{oc} = \frac{nkT}{q} \times \ln\left(\frac{I_L}{I_o} - 1\right) \tag{2.2}$$

The effect of the 45° tilt is also noticed in Figure 2.9. Ideally, the I-V curve of the PowerModule should correspond to the solid red line. However, this scenario will never represent in real-life since the the PowerModule is always angled at an angle of 45°. Consequently, the dotted blue, cyan and green show the expected behaviour since they correspond to scenarios with both 45° tilt angles and glass coverage. The window manufacturers prefer to have an anti-IR coating on the outside window so as to avoid excessive heat build-up inside the window and inside the house (low U-value). This coating is usually applied on the 1st glass, however, for optimal PowerWindow design in terms of power, this is not the best case. It is ideal to use clear glass since the loss in current and voltage is the least as compared to the other scenarios. Although, this is not the solution that Physee can use, it provides the maximum amount of power generation. As of now, Physee uses scenario 9 which uses is to strip off the anti-NIR coating from the glass after it has been placed through a mechanical etching process. It causes a loss of 39 % in I_{sC} and 3 % in V_{oc}, which is presented by the dotted cyan coloured line.

Figure 2.10 compares the ideal case power (scenario 1) to the power produced when the PowerModule is tilted at 45°, covered by glass. Again, scenario 9 (dotted cyan) represents the maximum power produced by the PowerModule. With respect to the ideal case, scenario 9 has a 39 % loss in the power produced as well. The difference in the losses in I_{sc}, V_{oC} and P_{mpp} with respect to ideal case (scenario 1) are presented in Table 2.7. The lowest loss in maximum power produced is in scenario 7 and the highest is in scenario 8. Therefore, an optimisation step for stripping the coating off of the clear glass is vital in order to increase the power production of the PowerModule by 10 % and reduce the loss from 39 % to 28 %.

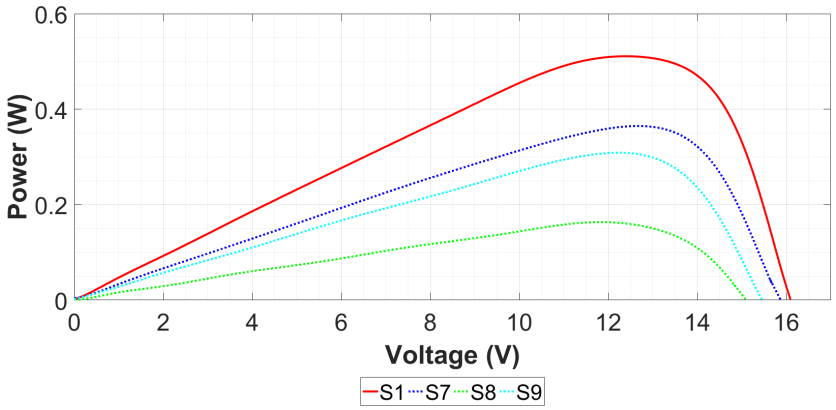

Figure 2.10: P-V curves for test case scenarios 1,7, 8 and 9 for one PowerModule where 'Scenario' is abbreviated to 'S'.

Table 2.7: Losses in I_{sc}, V_{oC} and P_{mpp} with respect to ideal case (scenario 1).

Scenarios	$\mathbf{I}_{sc}$ (%)	$\mathbf{V}_{oc}$ (%)	$\mathbf{P}_{mpp}$ (%)
7	28.08	0.44	27.68
8	65.21	5.07	67.44
9	39.13	2.9	39

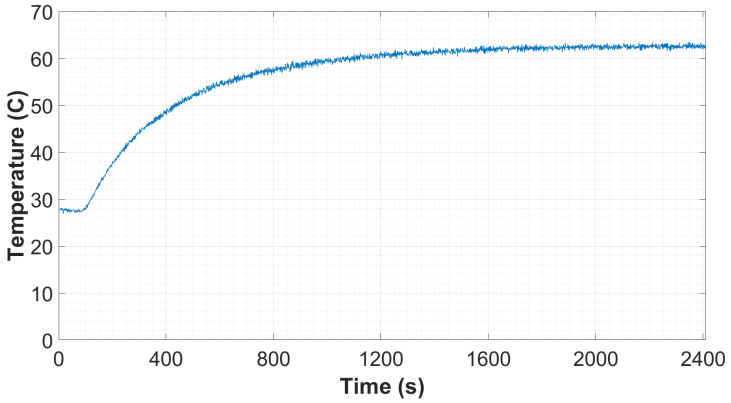

Figure 2.11: Temperature of the solar cell when the PowerWindow is kept under a LASS.

2.6. PowerWindow

2.6.1. Steady State Test

The Steady State test analyses the electrical behaviour of the Power Window an additional set of temperature dependent electrical measurements. The experiment was using a LASS at the EternalSun facility. It also estimates the DC power output of the PowerWindow at STC. The maximum power that a PowerWindow, with a stripped glass type, was found out to be 3.46 W at STC. Furthermore, to record the temperature of the solar cells, temperature sensors were placed under the solar cells in the PowerWindow. The temperature was recorded when the PowerWindow was kept under the solar simulator. It can be seen from Figure 2.11 that there exists an exponential delay of 33 minutes (≈ 2000 seconds) before the temperature of the solar cell stabilises. The maximum temperature reached by the solar cell is ≈ 62 °C at STC.

2.7. Conclusions

As mentioned at the start of the chapter, the aim of this chapter was to report the differences in the observed electrical values of the solar cells and modules to the ones claimed in the datasheet. This has been done and it was found that the electrical parameter values claimed in the datasheet were very different from those performed through experiments. Another goal was to understand the electrical behaviour of the PowerWin-

dow under solar simulators. Through different tests conducted in Section 2.5.1, it was observed that the DC power output is dependent on the glass type. It was concluded that an optimisation step was vital in the stripping of the anti-NIR coating from the glass to improve the performance of the PowerModule by 10 %. It was found that the PowerWindow produces a maximum power of approximately 3.5 W. Finally, the optical, opto-electronic and electrical parameters values such as the reflectance, current, voltage and so on were reported and will act as an input in the optical (Chapter 3), thermal (Chapter 4) and electrical (chapter 5) chapters to further characterise the PowerWindow.

3

Optical Modelling

An important step in the prediction of the energy yield, is the calculation of the irradiance incident on the surface of the PV module. The goal of this chapter is to calculate as well as evaluate the irradiance distribution for different PowerWindow (PW) orientations (e.g. north, south, east and west) and different geographical locations, which will serve as an input for thermal and electrical models next chapters. It is based on the model developed by Santbergen et al. [15] and performed using advanced optical ray tracing software called LightTools. The ray tracing software applies the principle of tracking individual ray paths from a light source to the PV module surface. As seen from the Figure 3.1, the optical model consists of two sub-models which are integrated together to obtain the incident irradiation, using equation 3.1.

$$Irradiation_{surface} = \int_{sky} (sensitivity\,map) \times (sky\,map)\, d\Omega \tag{3.1}$$

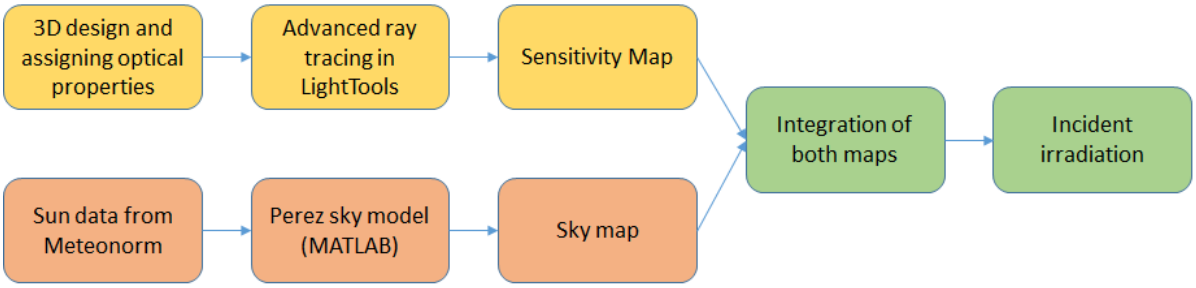

Figure 3.1: Optical model flow chart displaying different steps required for incident irradiation determination.

The first sub-model focusing on finding the sensitivty map (Section 3.0.2), while the second sub-model determines the sky map (Section 3.0.3). More information about models and their functioning can be found in the paper by Santbergen et al. [15].

This chapter aims to evaluate the following:

1. the effect of different orientations and tilts of the solar cells inside the PowerWindow;
2. the effect of placing the PW in different orientations;
3. the effect of shading on the PowerWindow by itself;
4. the effect of geography on the irradiance distribution of the solar cells inside the PowerWindow.

3.0.1. Simulated Sky Dome

Figure 3.2 represents a hemispherical sky dome that is discretized in equilateral triangles, where each triangle represents a set of azimuth and zenith angles. The light source created in LighTools is moved around

the object under simulation using such different sets of angles. This discretization by Regondi [28] is an improvement on the model by Santbergen et al. [15]. The sky dome can be discretized in number of triangles (40, 160, 640, etc.), and this number depends on how accurately one wants to simulate the hemisphere. The discretization of 640 triangles was chosen as it represented a good compromise between accuracy and computation time.

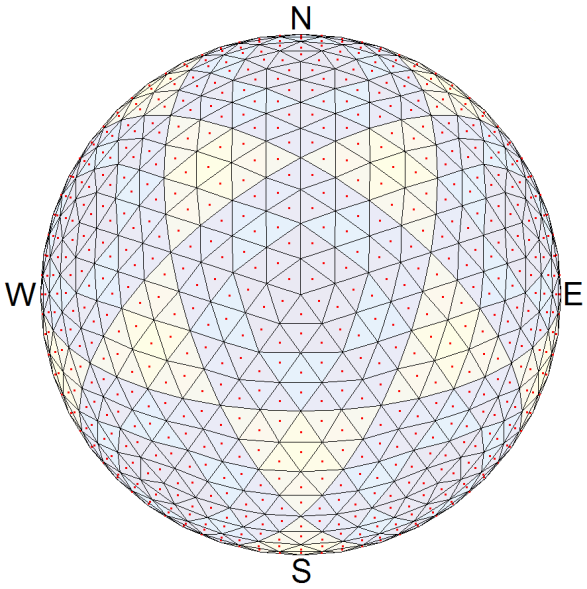

Figure 3.2: Top view of the sky dome discretized in 640 triangles.

3.0.2. Sensitivity Map

The data obtained after running the simulation on LightTools was processed in MATLAB and the sensitivity factor was computed. Equation 3.2 is used to obtain the sensitivity S of each PV surface [15].

$$S = \frac{P_{cell}}{A_{cell} \times I_{inci}} \tag{3.2}$$

Here, P_{cell} represents the data values incident power on the PV surface gathered from LightTools, A_{cell} is the area of that surface (= 0.000154 m^2) and the I_{inci} is the incident irradiance (= 1000 W/m^2). Figure 3.3 displays an example of a sensitivity map where each triangle represents a set of azimuth (*az*) and zenith (*ze*) angles. The black area in the map signifies zero sensitivity of a surface while the lower half of the map shows a non-zero sensitivity at different combinations of *az* and *ze* angles.

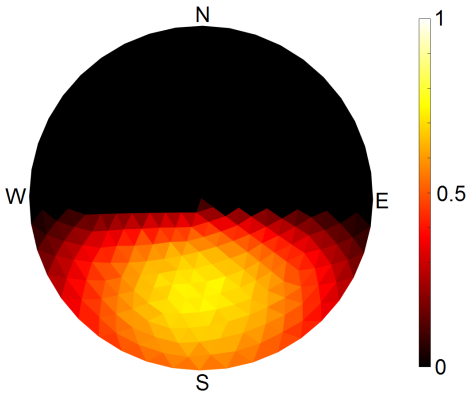

Figure 3.3: An example of a sensitivity map.

3.0.3. Sky Map

A sky map is a representation of the irradiance distributed across the entire sky using meteorological data [15]. It combines both the direct and diffuse component of irradiance in the sky, separately. The direct component is taken from the meteorological data and added to the sky element (triangle) that corresponds to the sun position at that time [15]. Whereas, the diffuse component is computed using the Perez model [16]. Both these models require the use of pre-existing meteorological data that is obtained from Meteonorm [29]. Example of two sky map, one sunny and one cloudy day, are displayed in Figure 3.4.

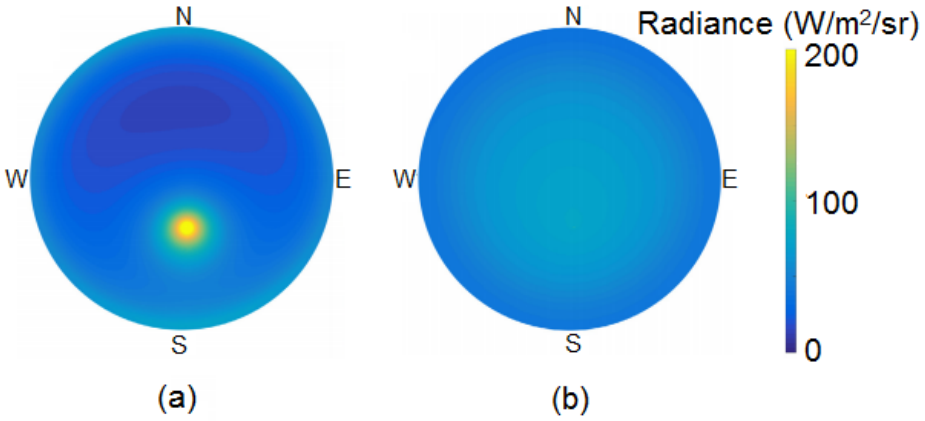

Figure 3.4: Examples of sky maps for (a) a sunny and, (b) an overcast day for the city of Eindhoven [15].

3.1. Simulation Input

The first sub model deals with calculation of the sensitivity map for each PV surface in the PowerWindow. The sensitivity map gives the information of the sensitivity of the surface to the incoming light for different sets of azimuth and zenith angles. In order to obtain this map, an advanced optical ray tracing simulation software called LightTools (LT) was used.

3.1.1. 3D Model

A 3D model of the PowerWindow was created in LightTools and each PV surface was assigned reflectance values of 5% based on the reflectance measurements shown in the previous chapter (Section 2.2.2). Similarly, each glass surface was assigned the property of being a smooth optical surface coupled with Fresnel loss. Additionally, a building structure behind the PowerWindow was constructed in order to mimic real life circumstances (Figure 3.5). A ground underneath the building structure was not simulated and therfore albedo was not taken into account.

3.1.2. Number of Rays

A PowerWindow consists of 288 PV cells each of area 1.54 cm^2. It is crucial to determine the appropriate number of rays R_n for the simulation that will provide the best trade-off between accuracy of the simulated irradiance value and simulation time.

In order to compute the appropriate R_n, a relative standard deviation analysis for the power incident on the surfaces was conducted for 5 different values of R_n. A reference surface (bottom cell) was taken into consideration and since the PowerWindow was oriented to the south, the sun was positioned in the south at an elevation angle of 40°. For each R_n, 10 sets of simulations were conducted by changing the set of random rays and the illumination area used was 1 m^2. The relative error was calculated by taking the ratio between the standard deviation and average value of the incident irradiation for these 10 simulations, calculated using equation 3.3. An acceptable relative error value for the case of the the PowerWindow can be < 1 %.

$$Relative\,error\,(\%) = \frac{Standard\,Deviation}{Average\,incident\,irradiation\,on\,cell} \times 100 \tag{3.3}$$

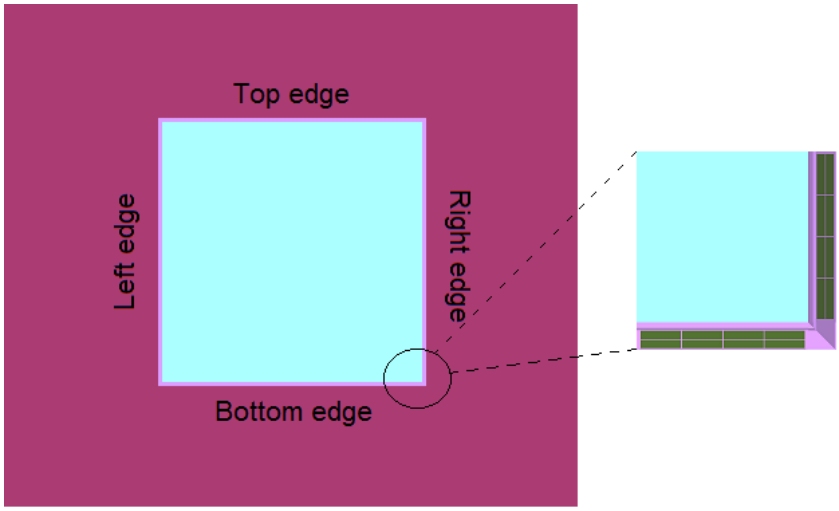

Figure 3.5: The model of a PowerWindow (in light blue and pink) with a building structure (maroon) behind it and a zoom-in of the cells (green) in LightTools.

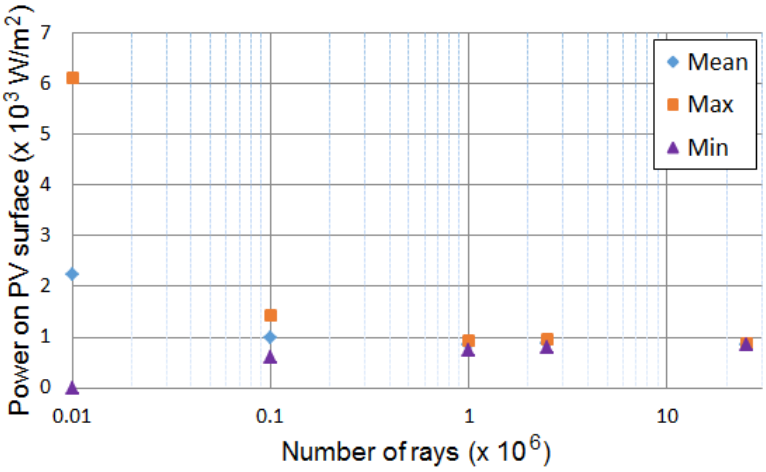

Figure 3.6: Power incident on the PV surfaces as a function of the number of rays used.

The irradiation was set to 1000 W/m^2 to mimic power delivered from AM1.5 [4]. When R_n was chosen as 10000, the average irradiation received on the reference PV surface was greater than 2000 W/m^2. This was because only a small fraction of the rays hit the PV surface and each ray carried more weight (in terms of power) as a result of low ray density. It can also be seen that the standard deviation in incident power was large. As R_n increased, so did the number of rays reaching the PV surface, reducing the standard deviation of the power incident on it. The average incident irradiation stablizes to a value of $\approx$ 855 W/m^2. This is seen in figure 3.6, where *mean*, *max* and *min* stand for mean, maximum and minimum value of power received by the surface in each of the 10 simulations.

Table 3.1: Error in irradiance as a function of number of rays used for simulation in LightTools.

R_n	Standard Deviation (W/m^2)	Relative Error (%)
10000	2651.99	244.52
100000	254.79	23.49
1000000	78.61	7.42
2500000	44.70	4.12
25000000	10.72	0.98

Table 3.1 displays both the standard deviation and relative error. It was observed that increasing R_n resulted in the decrease of the relative error. For 2.5 millions rays, the relative error was < 5 % which corresponds to a value of ≈ 45 W/m^2, whereas the relative error reduced to a more acceptable value of < 1 % (≈ 11 W/m^2) for 25 million rays. As a result, all following simulations presented in this chapter were conducted with 25 million rays. Since the discretization of 640 triangles was chosen, the total run time for each simulation for 25 million rays was 640 × 1 minute which was equal to ≈ 11 hours. Using 100 million rays would have significantly increased the simulation run time to more than 2 days per simulation with only a 50 % reduction in the standard deviation and relative error. Thus, 25 million was chosen as optimal solution for measurement needs.

3.2. Simulation Results

The results of the simulations will be analysed using different solar cells in the PowerWindow. These are numbered as shown in Figure 3.7.

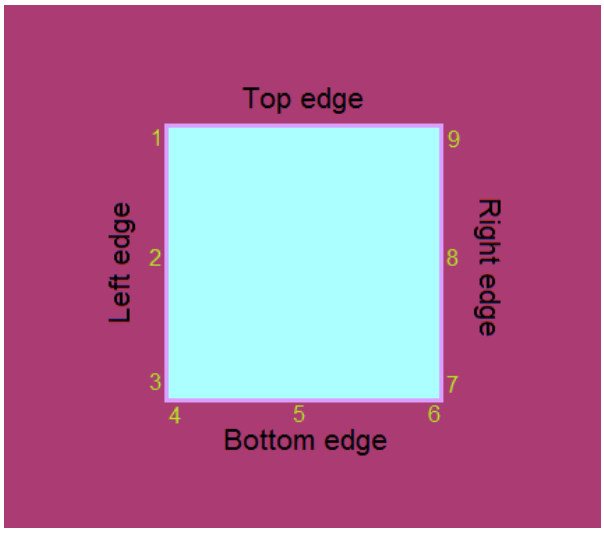

Figure 3.7: Numbering the cells used to analyse self-shading.

3.2.1. Effect of Differently Oriented and Tilted Cells Inside the PowerWindow

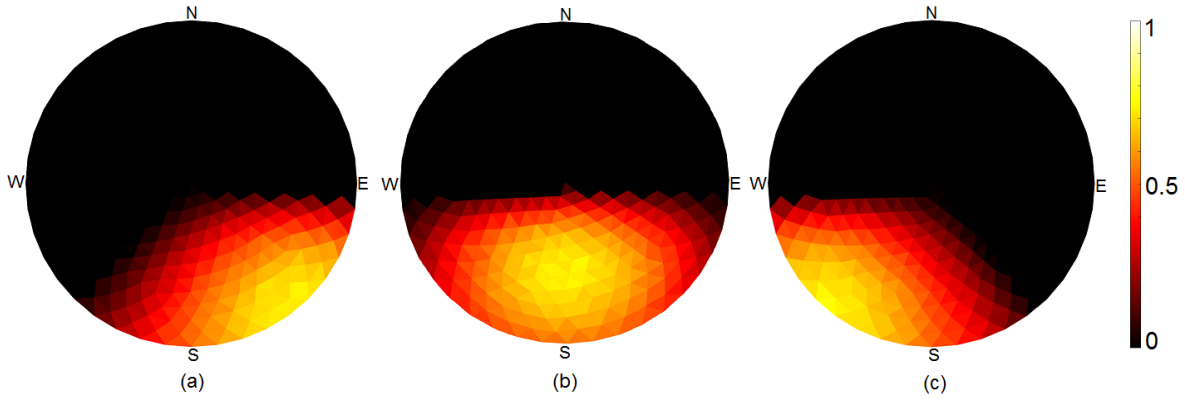

Figure 3.8: Sensitivity maps for (a) centre left (2), (b) centre bottom (5), and (c) centre right (8) cells.

The PowerWindow generates power from its edges by equipping the bottom edge with solar modules at a tilt angle of 45°, and the left and right edge with different orientations at a tilt angle of 90°. Consequently, each PowerBar, inside the window, is oriented in a different direction (as seen in introduction figure) and therefore, will be more sensitive to those directions. Three cells, one from the middle of each PowerBar, were

chosen in order to evaluate the effect of 'internal orientation' of solar cells inside the PowerWindow. These cells are named cells 2, 5 and 8 as seen in Figure 3.7. When a PowerWindow faces south, the cell 5 is sensitive primarily to the light from the south, as seen in Figure 3.8. Similarly, since the cell 8 and cell 2 are vertical (θ_C = 90°) and they are oriented towards south-west and south-east respectively, these cells are strongly sensitive to the light from those directions.

It should be noted that the sensitivity of a surface never reaches 1 because of reflection losses from the PV surface as well as Fresnel loss from the glass. Furthermore, for all three cases, the surfaces show zero sensitive to light from the north. This is due to the presence of the (simulated) building structure behind the PowerWindow in LightTools.

3.2.2. Effect of Self-Shading

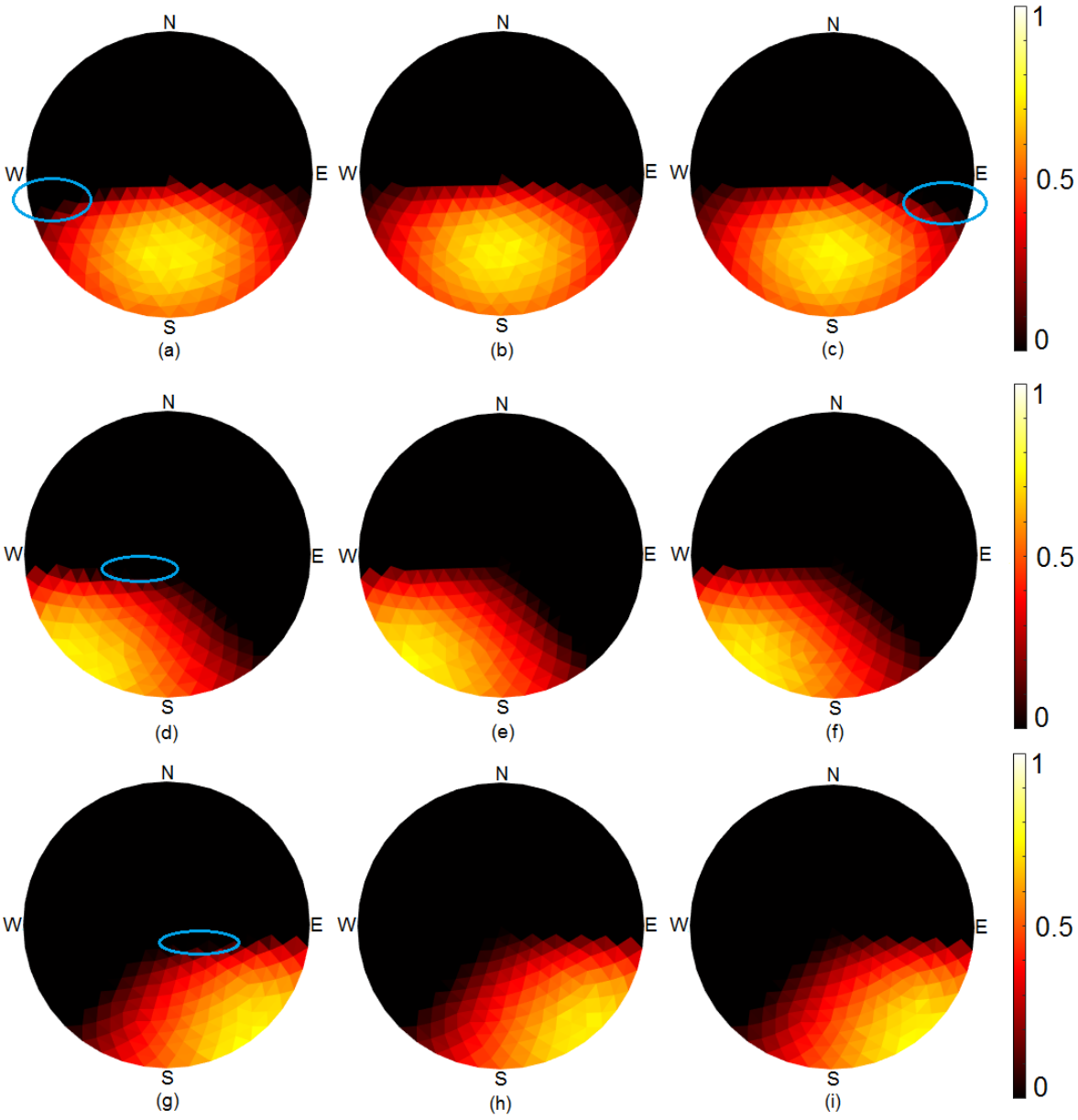

Figure 3.9: Sensitivity maps of cell number (a) 4 , (b) 5 , (c) 6, (d) 9, (e) 8, (f) 7, (g) 1, (h) 2, and (i) 3.

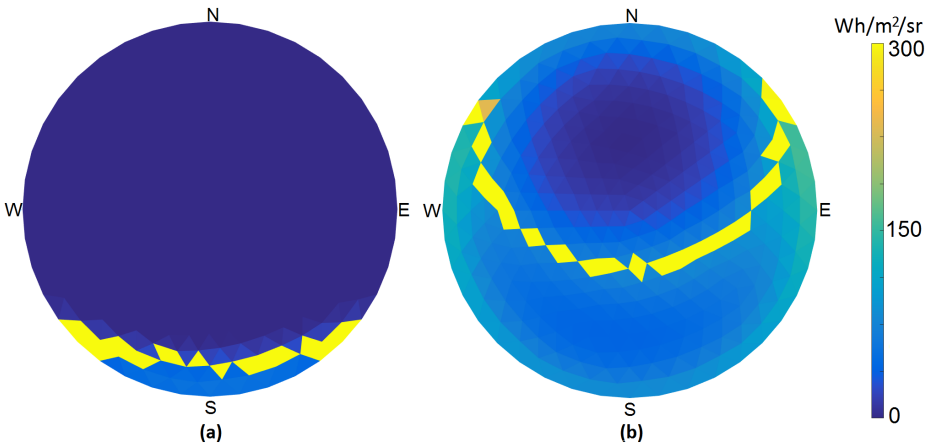

Figure 3.10: Sun path for (a) December 19 and (b) June 28 in Eindhoven shown in yellow.

A PowerWindow can cast a shadow on one of its PowerBars, and this phenomenon is called self-shading. It is important to evaluate the effect of the shade that the PowerWindow casts of itself since it will affect the total DC power output of the PowerWindow. A PowerBar in a 1 m^2 PowerWindow is made up of 4 parallel connected PowerModules. Each PowerModule has 24 series connected cells, and every 8 cells have a bypass diode to counteract external environmental shading. With the help of self-shading analyses, the number of bypass diodes as a result of self-shading can be determined. In order to understand the effects of self-shading of the PowerWindow, the sensitivity map of 9 specific cells will be analysed. The sensitivity map for 3 cells, 2 placed at the extreme edges and 1 in the centre (Figure 3.7), in each PowerBar were analysed. Figure 3.9 displays the sensitivity map of 3 cells in the bottom, right and left PowerBars, when the PowerWindow faces south.

For the bottom PowerBar, left-bottom (4), centre-bottom (5) and right-bottom (6) cells were taken into consideration. Their sensitivity maps are given in Figure 3.9 (a-c). It can be seen that the sensitivity maps of these cells are quite similar. However, for 4 and 6 cells it differs around the south-west and south-east side respectively. This is due to the internal shading effect of the edges of the PowerWindow on the bottom PowerBar. Consequently, this affects the sensitivity map. For the left and right PowerBar, top-left (1), centre-left (2), bottom-left (3), top-right (9), centre-right (8) and bottom-right (7) cells were taken into account respectively. It can be seen from Figure 3.9 (d-i) that only the *ze* sensitivity of 1 and 9 cells is affected by self-shading due to the top edge of the PowerWindow and there is no effect of the *az* sensitivity. This means that for high elevation angles of the sun, cells 1 and 9 will receive less irradiance compared to their respective counterparts. The effect of this self-shading can be studied by examining the sun path. To visualize this, the data for a summer and winter day was gathered for the city of Eindhoven. This location was chosen as the weather data were available from a previous project.

Bottom Cells

Figure 3.10 displays the sunpath for winter (December 19) and a summer (June 28) day. On the 19th of December, the sun rises in the south-east and sets in the south-west. The effect of self-shading, as depicted by the blue circles in Figure 3.9 (a) and (c), on the bottom cells does not bear any consequence on this day since the sun never reaches the circled blue positions in the sky on this day. Therefore, the incident irradiance on these bottom cells, as seen in Figure 3.11 (a), is similar. On the 28th of June, the sun rises in the north-east and sets in the north-west. On this day, not only does the sun rises rise in the north-east but also gains altitude as the day progresses, as seen in Figure 3.10. Since cell 6 shows zero sensitivity for north-east to around the east (see blue circle Figure 3.9 (c)), lower incident irradiance values are seen in figure 3.11 for this cell at that time. As the day progresses, on account of 6 cell's sensitivity map, it receives almost the same amount of irradiance as cells 4 and 5 until around 3:30 pm. At this time, the sun is in the blue circle shown in Figure 3.9 (a). The lack of sensitivity for both the *az* and *ze* angles in cell 4 starts showing its effects. Between 3:30 - 4:30 pm, cell 4 receives 50 % less irradiance than its counterparts.

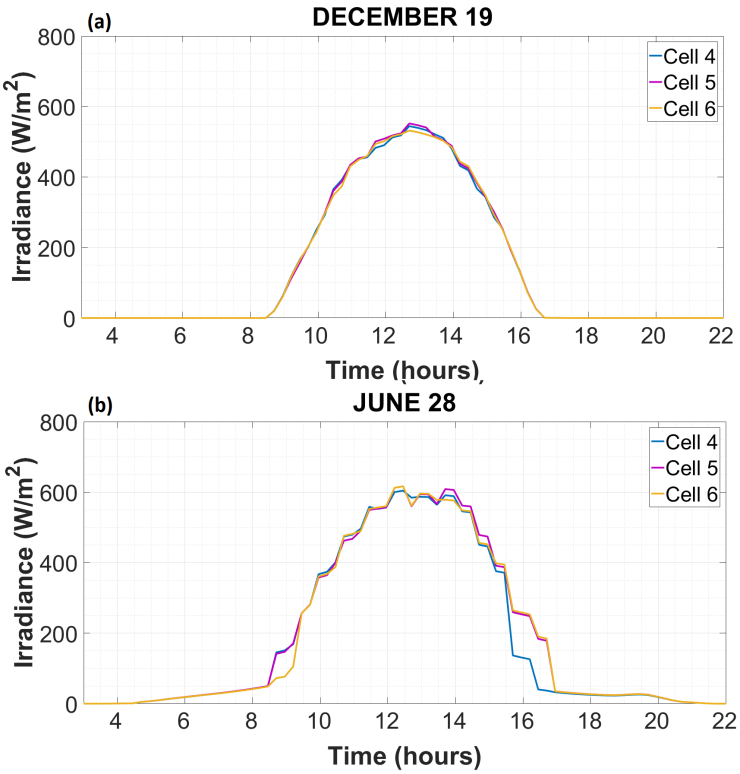

Figure 3.11: Irradiance profile for cell number 4, 5, and 6 for (a) December 19 and (b) June 28 in Eindhoven.

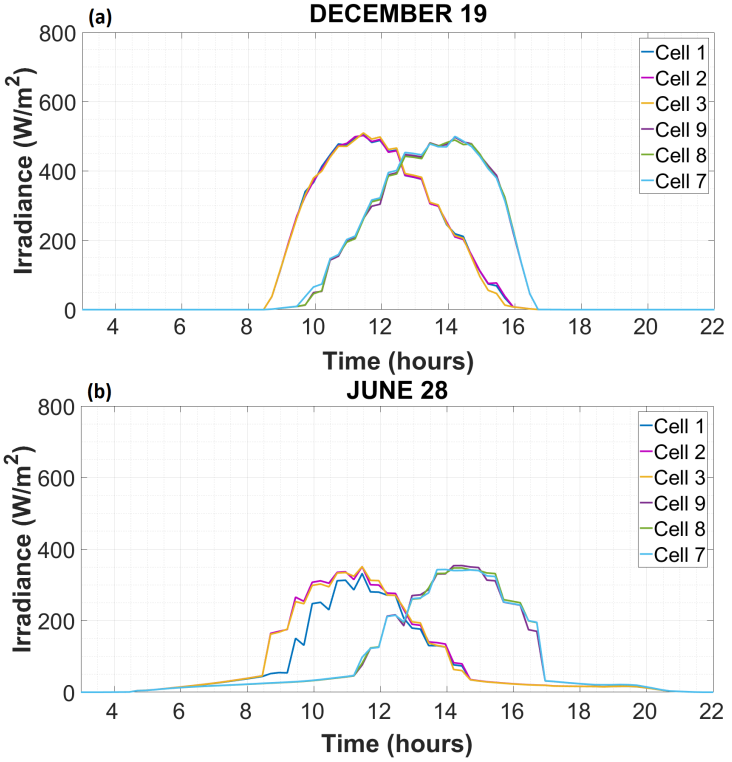

Figure 3.12: Irradiance profile for cell number 1, 2, 3, 9, 8 and 7 for (a) December 19 and (b) June 28 in Eindhoven.

Left and Right Cells

The sun is closer to the horizon on the 19th of December, and thus, the irradiation received by the left and right cells is almost similar, as seen in Figure 3.12 (a). However, for June 28th, the 1 cell receives an average of 71 % less irradiance than 2 and 3 cells till noon (Figure 3.12 (b)). This is because the sun (Figure 3.10 (b)) is very close to the blue region shown in Figure 3.9 (g). The same trend for cell 9 is not seen because the sun is not very close to the blue circle seen in Figure 3.9 (d) and available irradiance reduces as the day progresses. Cell 9 receives on average 10 % less irradiance as compared to cells 7 and 8.

3.2.3. Effect of the Orientation of the PowerWindow

The aim of this study was to understand and report the difference in the irradiation received by the PowerWindow when placed in north, east, west, and south. Again, for the sake of visualisation, the data was gathered for cells 2, 5 and 8 since the PowerWindow is symmetric. The orientation of the PowerWindow was changed in LightTools and the same simulations were conducted.

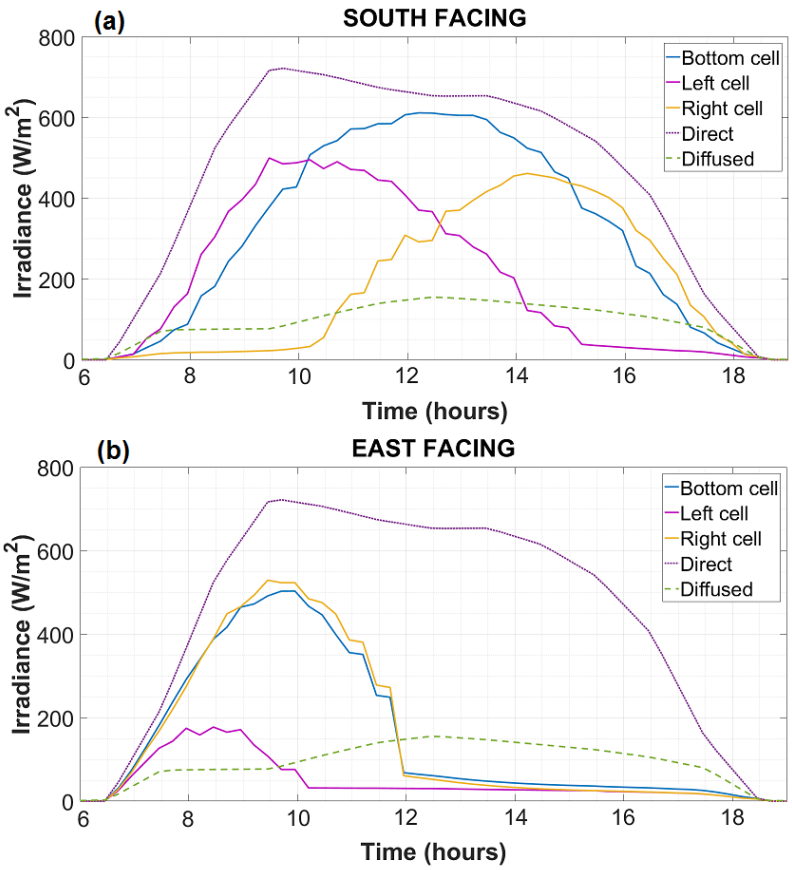

Figure 3.13: Irradiance versus time graph for the 21st September for (a) south and (b) east facing PowerWindow.

South

When the PowerWindow is oriented south (Figure 3.13 (a)), all three cells are active during the day i.e. they receive irradiance. The bottom cell receives the highest amount of irradiation and it peaks around when the irradiance is the highest throughout the day, which is around 1 pm and when the sun is in the south. Even though the left and the right cells receive irradiation throughout the day, it is clear from Figure 3.13 that they receive maximum irradiation at different times of the day. The left cell receives higher irradiation in the morning, while the right cell receives higher irradiation in the late afternoon to evening. This clearly shows that all three cells are most active in different parts of the day. This result is in accordance with the sensitivity information presented in Section 3.2.1. It should be noted that the difference in the peak irradiance values of the left and right cells is because, on this day, there is more irradiation in the morning than in the evening

(according to meteonorm data) [29].

It is evident from Figure 3.14, that the bottom cell receives the highest irradiation throughout the year. The solar radiation on a photo-voltaic surface is dependent on the angle of incidence (AOI) on that surface. This irradiance is dependent on the orientation of the PV surface and its tilt. If the tilt of the PV surface is fixed, the AOI on that surface is subjected to change as the path of the sun changes throughout the year. Similarly, if the tilt of the PV surface changes with respect to sun position, it will receive maximum solar radiation [4].

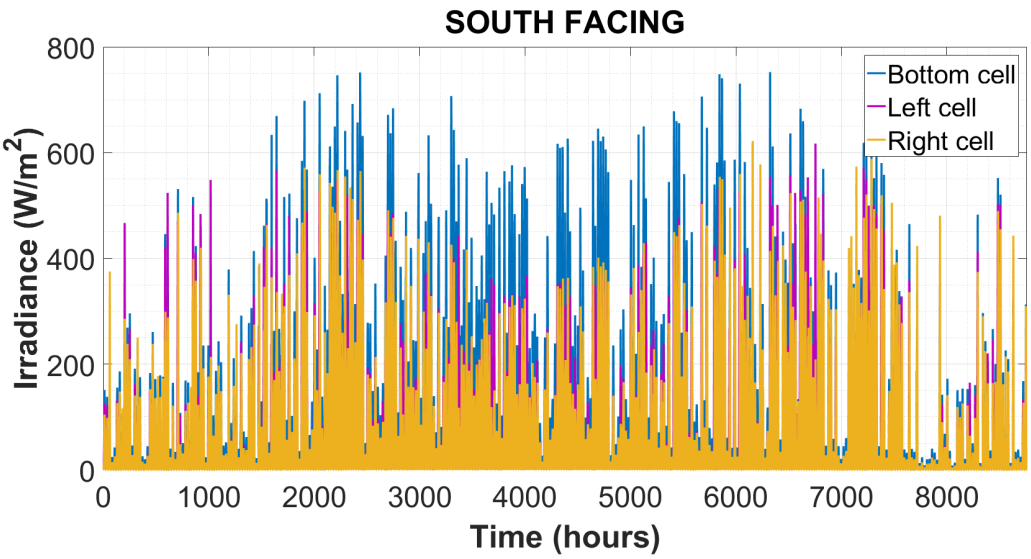

Figure 3.14: Plot of irradiation versus time for a Powerwindow placed in the south in LT.

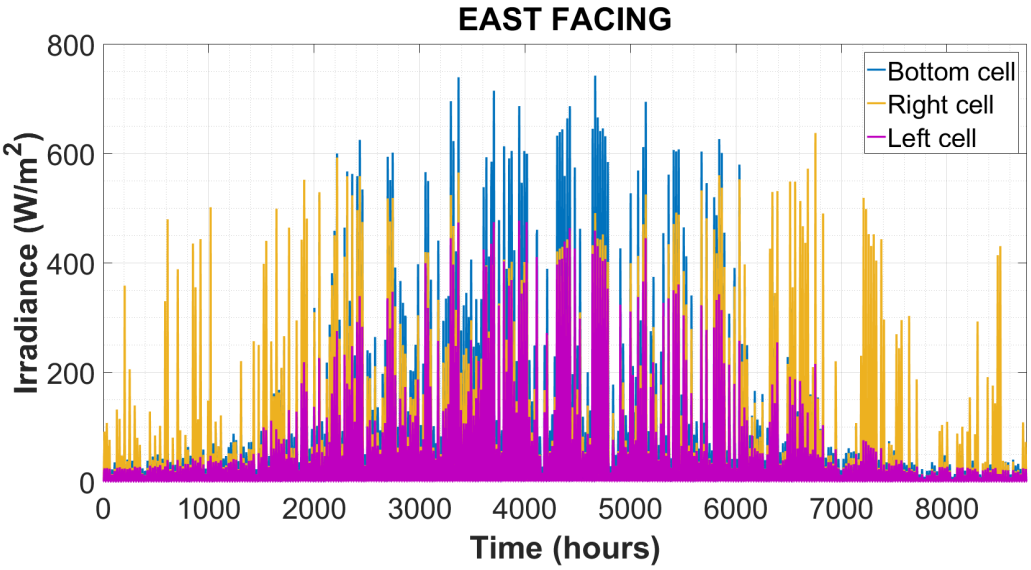

Figure 3.15: Plot of irradiation versus time for a Powerwindow placed in the east in LT.

East

When the PowerWindow is oriented towards the East, according to the sensitivity maps, the left cell is oriented towards the north-east, the bottom towards the east and right towards the south-east. The right cell receives the highest amount of irradiation on this day followed by the bottom cell and then the left cell (Figure 3.13 (b)). When the sun crosses the south, the left cell ceases to receive direct irradiance. When the sun

reaches the south, the entire PowerWindow stops receiving direct sunlight. The incident irradiance drastically drops on the bottom and right cells. All receive less than 100 W/m^2 at noon to a value that eventually drops to lower values as the day progresses. This is as a result of diffused irradiance.

Figure 3.15 (b) displays the yearly irradiation incident on the 3 cells. In general, in the northern hemisphere, the elevation angle of the sun in the winter months is closer to the horizon [4]. It can be observed that even though the bottom cell receives the highest amount of irradiation throughout the year, the right cell receives either equal to or slightly more irradiation in the winter months (end of September to end of March) as compared to the bottom cell. This is due to the internal orientation of the right cell, as its sensitivity is maximum at the horizon of the south-east direction.

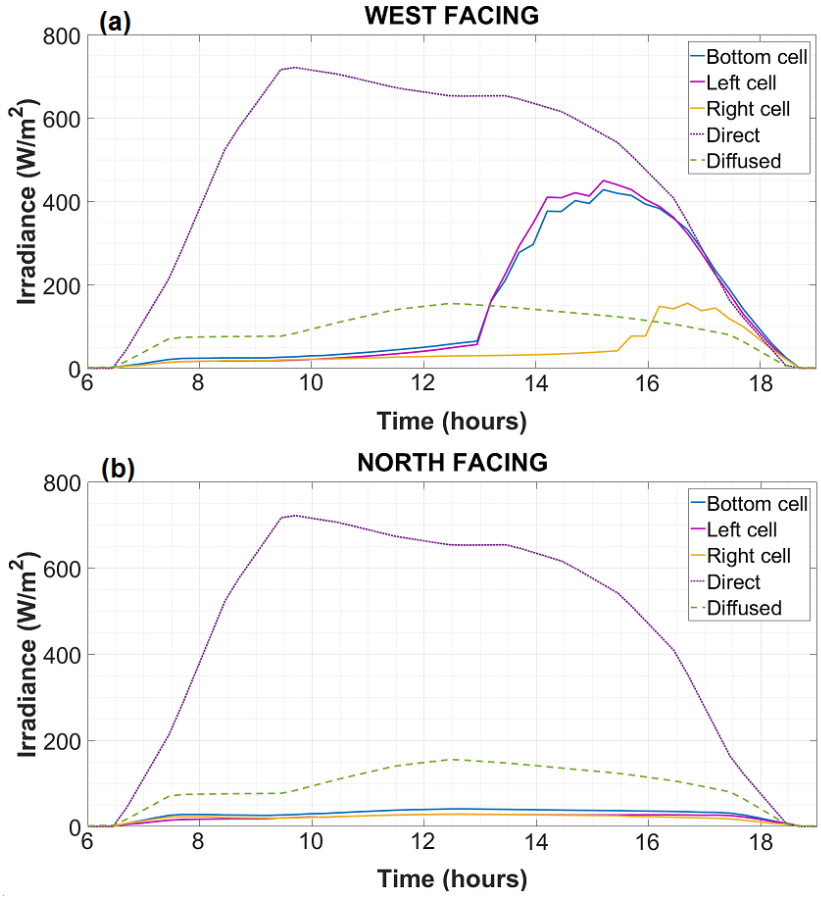

Figure 3.16: Irradiance versus time graph for the 21st September for (a) west and (b) north facing PW.

West

The opposite trend is seen for a west facing PowerWindow (Figure 3.16 (b)) as compared to the east facing PowerWindow. Here, the bottom cell faces the west, the left cell faces the south-west, while the right cell faces north-west. Consequently, after the sun crosses the south, there is a sudden increase in the irradiance incident on the bottom and left cell. When the sun crosses the south-west, the right cell starts to receives direct irradiance.

According to Figure 3.17, the left cell receives the equal to or slightly higher amount of irradiance in winter months as compared to the bottom cell. The explanation is similar to that provided in Section 3.2.3. However, the left cell receives less irradiation as compared to right cell when PowerWindow faces the east as mentioned in Section 3.2.3. This is because of the intensity of sunlight available in the afternoon-evening is less than in the morning-noon time [29].

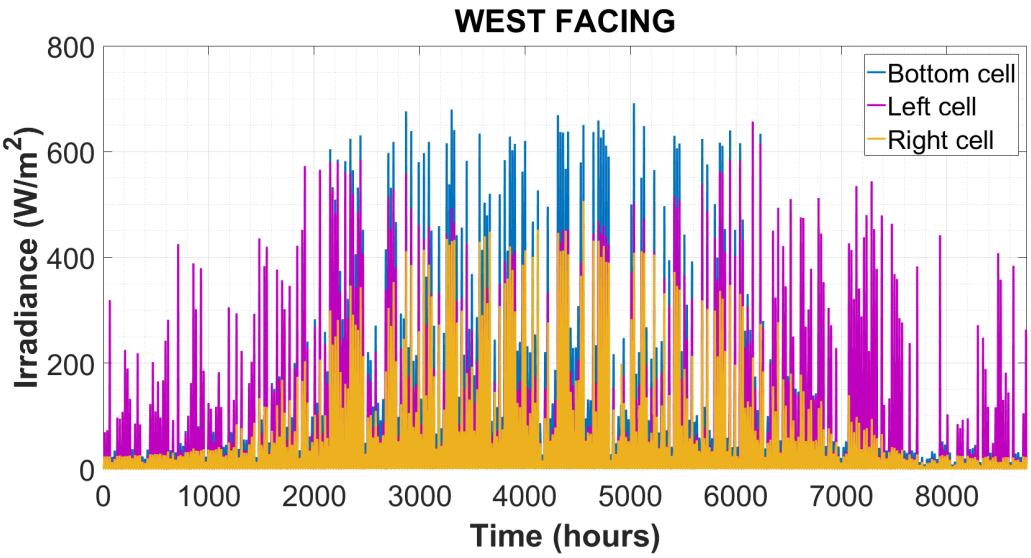

Figure 3.17: Plot of irradiation versus time for a Powerwindow placed in the west in LT.

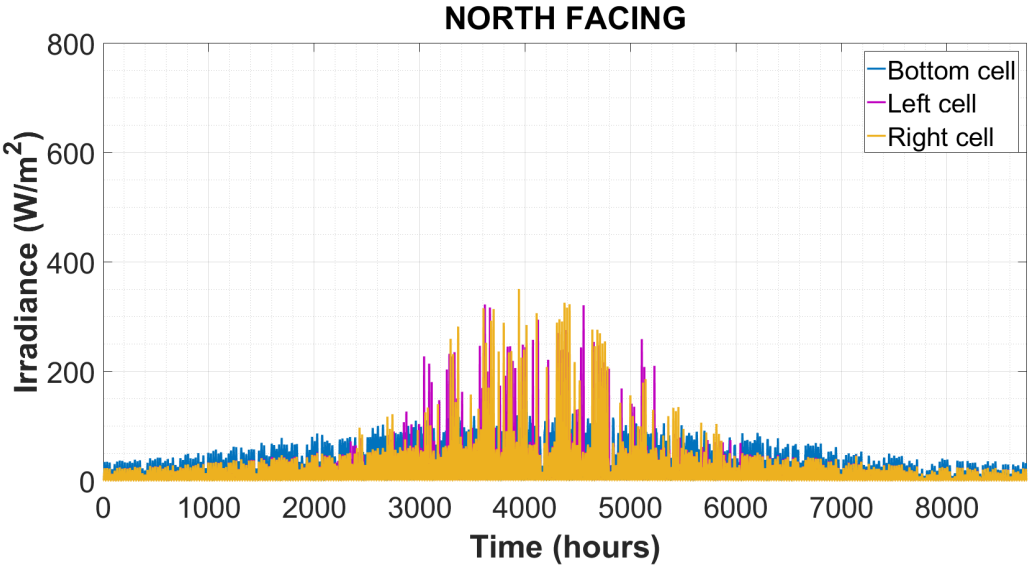

Figure 3.18: Plot of irradiation versus time for a Powerwindow placed in the north in LT.

North

A north facing PowerWind receives irradiance less than 50 W/m^2 as seen in Figure 3.16 (a). In this case, the bottom cell faces the north, the left cell faces north-west and the right cell faces north-east. Since Eindhoven is located in the Northern hemisphere, there is no direct sunlight coming from the north. Therefore, the cells in the PowerWindow receive diffuse sunlight throughout the day. Even in this case, the bottom cell receives more irradiance than the other two cells as a consequence of its sensitivity map.

A north facing PowerWindow also receives some amount of incident irradiance throughout the year as seen in Figure 3.18. For the summer months, the cells receive almost 4 times the irradiation as much compared to the rest of the year. This can be explained by the sun-path given in Figure 3.10 (b). In the summer, the sun rises in the north-east and sets in the north-west. Therefore, the left and right cells receive more irradiation as compared to the bottom cell because of their internal orientation.

3.2.4. Effect of Geography

When the PowerWindow is placed in different locations, as mentioned in section, the AOI of sunlight changes with respect to the sun's position in the sky. In this study two locations, Palermo and Dubai, other than Eindhoven were chosen to demonstrate the difference in the irradiance profile on the solar cells when placed in these cities. Since all these cities have a different geographical location in the northern hemisphere, the path that the sun takes through out the year varies for each city. This is shown in Figure 3.19.

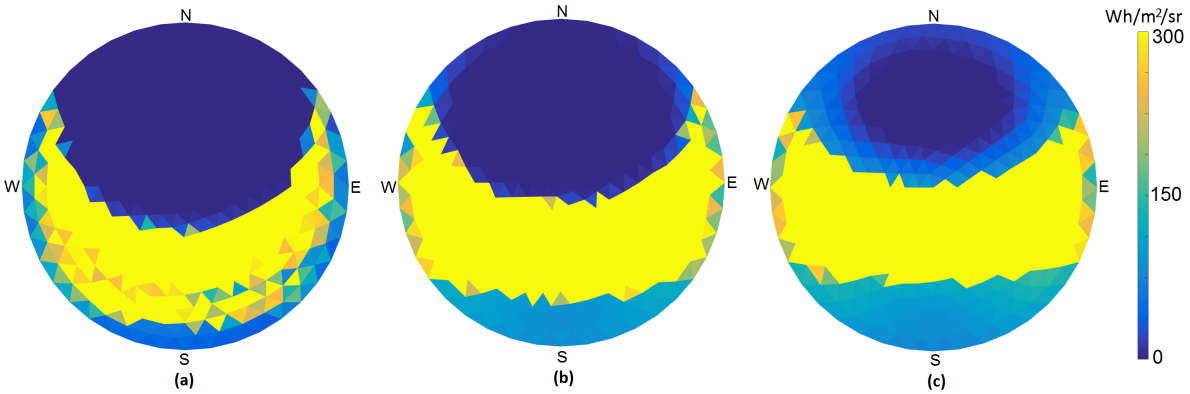

Figure 3.19: Integral sky map of the sunpath throughout the year for (a) Eindhoven, (b) Palermo, and (c) Dubai.

The integral sky map is a combination of the sun's position throughout the year as well as diffused distribution of light in the sky for a particular location[1]. In Figure 3.19, the yellow portion marks the position of the sun in the sun (blue portion) throughout the year. It can be seen from integral sky maps (Figure 3.19) that altitude of the sun is lowest for Eindhoven and closest to the horizon during the year. The sun's lowest altitude is higher for Palermo than Eindhoven and is the highest for Dubai. Furthermore, the highest altitude of the sun during the year is the greatest for Dubai, followed by Palermo and then by Eindhoven.

Only the south facing orientations when the PowerWindow is placed in different locations are used to describe the effect of geography on the irradiance profile on the solar cells. Figures 3.14, 3.20 and 3.21 give the irradiance distribution on the cell numbers 5, 2 and 8 respectively. It is evident from these images that all three cities have very different irradiance distribution profiles throughout the year due to the difference in the sunpath in these locations. Even though the irradiation received in Dubai is greater than that in Palermo and Eindhoven, the incident irradiation on the cells during the summer months for Dubai is the lowest. This is due to the un-optimized tilt of the cells inside the PowerWindow. Palermo receives the highest amount of incident irradiation owing to the amount of irradiation available in this location and because the tilt angle of the bottom PowerBar is closer to the optimum tilt angle required for Palermo. Additionally, lowest altitude of the sun is closer to the horizon for Palermo than for Dubai and thus, the centre left and centre right cells receive higher incident light in Palermo than in Dubai. After Palermo, Dubai receives the highest amount of irradiation, followed by Eindhoven.

[1] Due to low resolution of the integral sky map, the analemma for the respective cities is not clearly seen. Therefore, for the sake of simplicity, the lowest curve of the yellow band seen in Figure 3.19 has been taken as the lowest point of the analemma during the year.

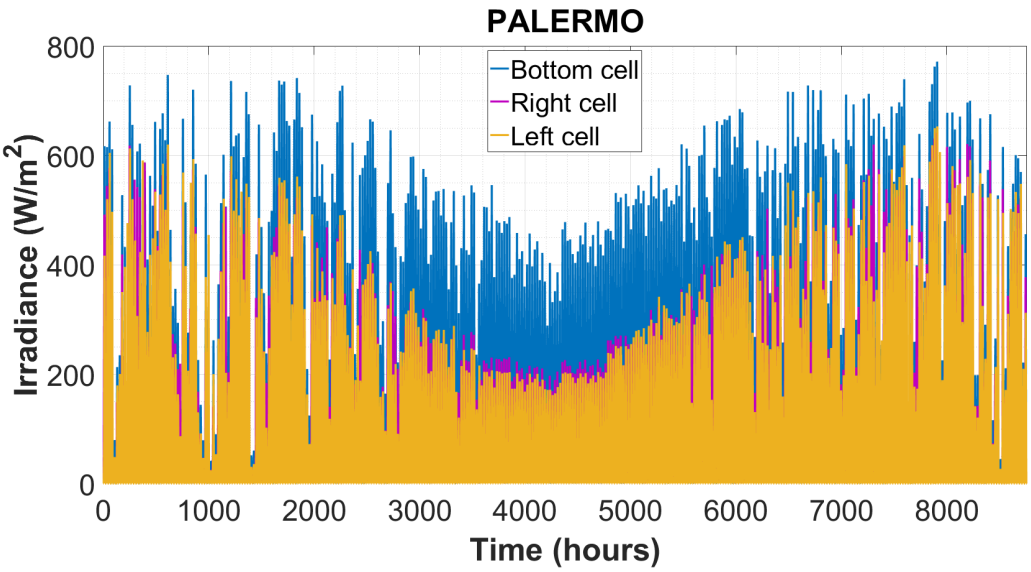

Figure 3.20: Plot of irradiation versus time for a Powerwindow placed in the south in the city of Palermo, Italy.

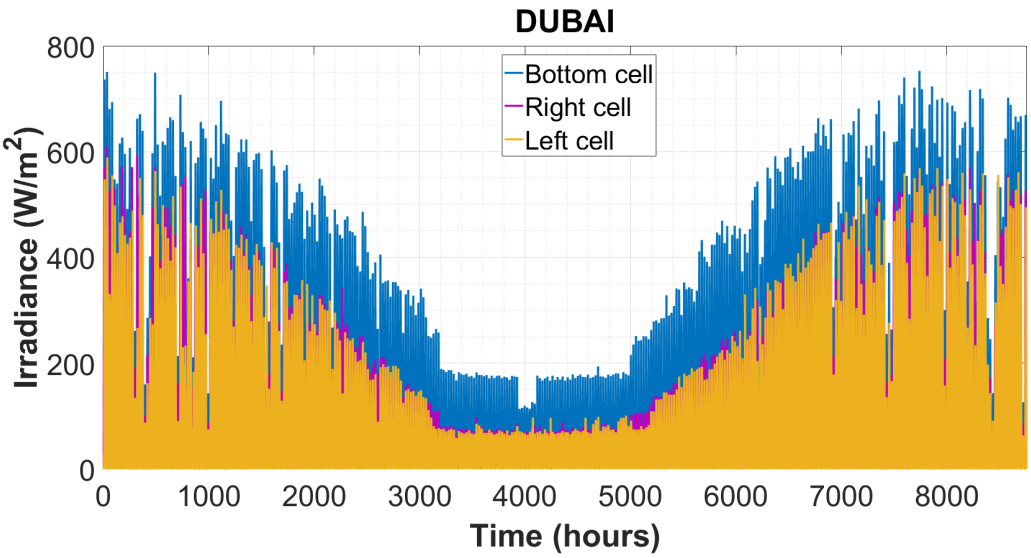

Figure 3.21: Plot of irradiation versus time for a Powerwindow placed in the south in the city of Dubai, UAE.

3.3. Conclusions

The aim of this chapter was to calculate and evaluate not only the irradiation distribution for different window orientations (north, south, east and west) and the different geographical locations such as Eindhoven, Palermo and Dubai. It also evaluated the effect of 'internal orientation' of the solar cells inside and self-shading of the PowerWindow.

Section 3.2.1 evaluates the effect of different orientations and tilts of the cells inside a PowerWindow. It was found that sensitivity maps of all three cells are very different from each other. Section 3.2.2 evaluated the self-shading of the PowerWindow and for this study a total of 9 cells, three cells from each PowerBar, were chosen. It was noted that the effect of self-shading was minimum for winter months and maximum for summer months. It was concluded that for the entire year, the effect of self-shading was small. Section 3.2.3 described the effect of placing the PowerWindow in different orientations on 1 cell from each PowerBar. It was noted that the south facing PowerWindow received the most amount of light while the north facing PowerWindow received the least. Section 3.2.4 analysed the effect of placing the PowerWindow facing south

in Eindhoven, Palermo and Dubai. It was found that irradiance distribution profile for each city was different as a result of the sun position throughout the year and the intensity of light received in each location.

The total incident irradiation on the PV surfaces for Eindhoven, Palermo and Dubai was estimated and their irradiance distribution profiles were evaluated. These irradiance values will serve as the input to thermal as well as electrical model presented in the next chapters.

4

Thermal Modelling

The accurate prediction of the energy yield of the PowerWindow entails the calculation of the solar cell temperature under operating conditions. Different methods have been developed and used to estimate the temperature of solar modules [18, 31, 32] but are not suitable in this case. The case of the PowerWindow poses a unique challenge since solar cells are placed inside a window envelope. These models do not assume cells to be placed inside windows. Consequently, it is necessary to develop a thermal model that gives a good estimate of the temperature of the solar cells inside the PowerWindow.

The goal of this chapter is to develop a thermal model for the cells in the PowerWindow. The ambient temperature values were taken from Meteonorm, while the irradiance values were estimated using LightTools in optical modelling chapter. This model requires as inputs the irradiance incident on the solar cell as well as the ambient temperature. The objectives of this chapter are as follows:

1. to develop a thermal model that can predict the temperature of every solar cell in the PowerWindow for every hour of the year;
2. To compare the Nominal Operating Temperature (NOCT) model with the Modified Fluid-Dynamic model modified for the PowerWindow;

The temperature values obtained from the thermal model will act as input to the final electrical model that will be discussed in the next chapter.

4.1. Nominal Operating Cell Temperature (NOCT) model

The NOCT model is the most widely used (even commercially) on account of its simplicity, however there is a trade-off with respect to its accuracy [4].

$$T_{cell} = T_{ambient} + \frac{T_{NOCT} - 20^{\circ}}{800} \times G \tag{4.1}$$

where, G is the incident irradiance on the solar cell per square meter. As seen from equation 4.1, this formula does *not* include wind-speed and other external parameters that may have an influence over the cell temperature.

4.2. Modified Fluid-Dynamic (MFD) model

The heat transfer mechanism of the solar cell temperature can be modelled as a function of its surroundings. Sandia National Laboratories (SNL) developed an approach to accurately model the solar cell temperature using available module parameters and weather data [18]. A simplified version of this model by Smets et al. [4] assumes steady state conditions.

Conventional heat transfer models cannot be applied directly to the PowerWindow where the PV cells are located in an air environment between two glass panes, tilted 45 relative to the glass. Therefore, for the sake of simplification, the heat transfer equations for a solar cell inside the PowerWindow have been taken into

consideration.

This model assumes the following conditions while calculating the temperature of the solar cell for each time-step:

1. The solar cell is a considered to be a single uniform mass;
2. No heat exchange takes place between the cell and Printed Circuit Board (PCB);
3. The ambient temperature is the same on all the sides of the module;
4. Steady State condition is assumed;
5. The ambient temperature outside is assumed to be the same inside the window.

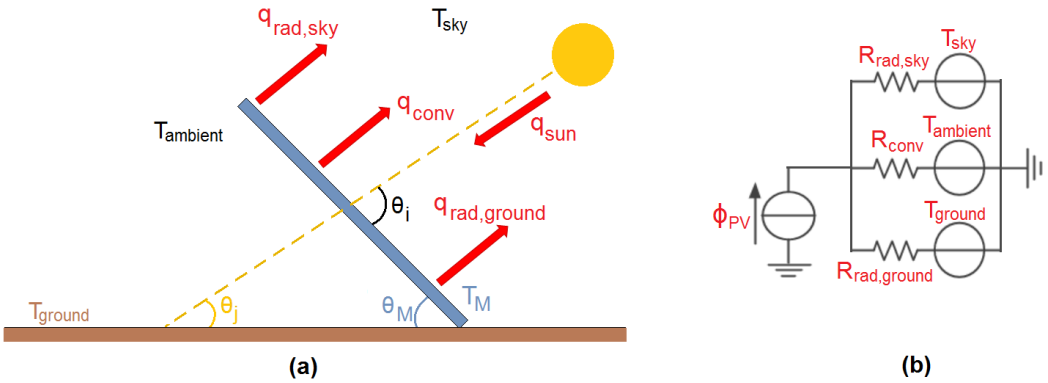

Figure 4.1: (a) Net heat exchange between tilted solar cell inside PowerWindow and its surroundings, and (b) equivalent thermal circuit network.

It should be noted that the PCB, over which the cells are soldered, is a poor conductor of heat[1]. As a result, the PCB is a thermal insulator and is unable to conduct heat away from the solar cell. Moreover, the contact point between the PCB and the aluminium frame is almost equal to the thickness of the solar cell (2 mm), which is very small. The net amount of heat taken away from the PCB to the aluminium frame is negligible. Therefore, heat transfer through conduction from the solar cell to PCB and PCB to aluminium frame is not taken into consideration. As a result of the assumptions, the heat transfer mechanism can be simplified to an equivalent thermal circuit network. The solar cell inside the PowerWindow radiates heat to the sky and ground, and loses heat through natural convection to the ambient air, as seen in Figure 4.1. Since there is no wind inside the gap of the windows, there is no forced convection. Also, the solar cell receives a heat flux when it absorbs incoming solar irradiation.

The time-step between irradiation values is 1 hour, and the cell temperature changes insignificantly as compared to the irradiation for such short time periods like 1 hour. This is because the cell temperature is slightly overestimated with increasing and underestimated with decreasing irradiance. These small deviations tend to cancel during the day [34]. It was found from the steady state experiments that the temperature of the solar cell stabilises after approximately 30 minutes. Consequently, the solar cell is considered to be in steady-state condition. The thermal energy balance of the solar cell for steady state conditions, as stated by the first law of thermodynamics, can be represented as shown in equation 4.2.

$$Q_{in} = Q_{out}. \tag{4.2}$$

Here Q_{in} represents the heat supplied to the cell, and Q_{out} the heat released by the cell.

The steady state equation for heat transfer for the solar cell inside the PW are presented in equation 4.3.

$$0 = h_c(T_{PV} - T_{amb}) + \epsilon_{top}\sigma(T_{PV}^4 - T_{sky}^4) + \epsilon_{back}\sigma(T_{PV}^4 - T_{ground}^4) - \phi_{PV}A_{PV} \tag{4.3}$$

[1] This is because it is made up of a material called FR-4 with a low thermal conductivity of 0.3 W/mK [35].

In equation 4.3, the first term, on the right hand side, $h_c(T_{PV} - T_{amb})$ is the total convective heat transfer, where h_c and T_{amb} is the total convective heat transfer coefficient for the solar cell and ambient temperature respectively. The second and third term $\epsilon_{top}\sigma({T_{PV}}^4 - {T_{sky}}^4)$ and $\epsilon_{back}\sigma({T_{PV}}^4 - {T_{ground}}^4)$ are the radiative heat transfer to the sky and ground respectively. Here ϵ_{top} and ϵ_{back} are the emissivity of the top and bottom surface of the solar cell respectively, σ is the Stefan-Boltzmann's constant and, T_{sky} and T_{ground} are the sky and ground temperatures respectively. These temperatures are calculated as stated in equations 4.4 and 4.5 [18].

$$T_{sky} = 0.0552 \times T_{amb}^{3/2} \tag{4.4}$$

$$T_{ground} = T_{amb} \tag{4.5}$$

Finally, the fourth term ϕA_{PV} is the heat flux as absorbed by the solar cell a result of irradiation incident on it, where ϕ is the product of absorptivity (α) of the solar cell and G. Further simplification of equation 4.3 can be done by linearizing the radiation terms using the formula mentioned in equation 4.6.

$$(x^4 - y^4) = (x^2 + y^2)(x + y)(x - y) \tag{4.6}$$

Even for a 10 °C change in cell temperature, the term $({T_{sky}}^2 + {T_{ground}}^2)(T_{sky} + T_{ground})$ varies by less than 5%. Consequently, this term is assumed to be constant [18]. Therefore, the linearized radiative terms hold the form as shown in equations 4.7 and 4.8.

$$H_{rad,PV,sky} = \epsilon_{top}\sigma(T_{PV}^2 + T_{sky}^2)(T_{PV} + T_{sky}) \tag{4.7}$$

$$H_{rad,PV,ground} = \epsilon_{back}\sigma(T_{PV}^2 + T_{ground}^2)(T_{PV} + T_{ground}) \tag{4.8}$$

By substituting equations 4.7 and 4.8 in equation 4.3, a linearized expression of the heat transfer equation for the solar cells inside the PowerWindow can be obtained as shown in equation 4.9.

$$\phi_{PV} A_{PV} = H_{conv,PV,amb}(T_{PV} - T_{amb}) + H_{rad,PV,sky}(T_{PV} - T_{sky}) + H_{rad,PV,ground}(T_{PV} - T_{ground}) \tag{4.9}$$

Equation 4.9 can be rearranged to calculate T_{PV} as shown in equation 4.10.

$$T_{PV} = \frac{H_{conv,PV,amb}T_{amb} + H_{rad,PV,sky}T_{sky} + H_{rad,PV,sky}T_{ground}}{H_{conv,PV,amb} + H_{rad,PV,sky} + H_{rad,PV,ground}} \tag{4.10}$$

As seen from equations 4.7 and 4.8, $H_{rad,PV,sky}$ and $H_{rad,PV,ground}$ are dependent on T_{PV}. Thus, equation 4.10 needs to be solved iteratively. This can be achieved by initialising the ambient temperature outside and calculating the all heat transfer equations individually inside the iteration loop.

4.3. Evaluation of models

The MFD model uses heat transfer equations that are tailor made for the solar cells inside the PowerWindow. The NOCT model, on the other hand, is an approximation based on average equilibrium temperatures of a PV cell when incident with an irrdiation of 800 W/m^2 at an ambient temperature of 20°. The external parameters that influence the temperature of PV cells are incident irradiance, ambient temperatures, and wind-speed. In the case of the PowerWindow, the solar cells are not directly exposed to the wind and therefore, forced convection is not taken into account in the modified fluid dynamics model.

In Figure 4.2, T_{amb} is the ambient temperature that is obtained from meteonorm [29] while the irradiance incident on the cell is obtained from the optical simulations explained in the previous chapter. T_{cell}*(MFD)* and T_{cell}*(NOCT)* represent the temperature of the cell simulated by the MFD and NOCT models respectively. It is visible this figure that the profile (shape) of cell temperatures is strongly dependent on the irradiation incident on the solar cell. This means that the higher the incident irradiance on the PV cells, the higher will be the PV cell temperature. As expected, during daytime the MFD model predicts a cell temperature that is higher than the temperature predicted by the NOCT model. For this day the difference is up to 9°C. Furthermore, unlike temperature obtained by the NOCT model, the temperature obtained from the MFD model falls below T_{amb} when the incident irradiation drops drastically. At this point, the incident irradiance is low and, according to the MFD model, the cell radiates heat to the sky while receiving heat from the ambient environment and ground through convection and radiation respectively. This is because the sky temperature (T_{sky})

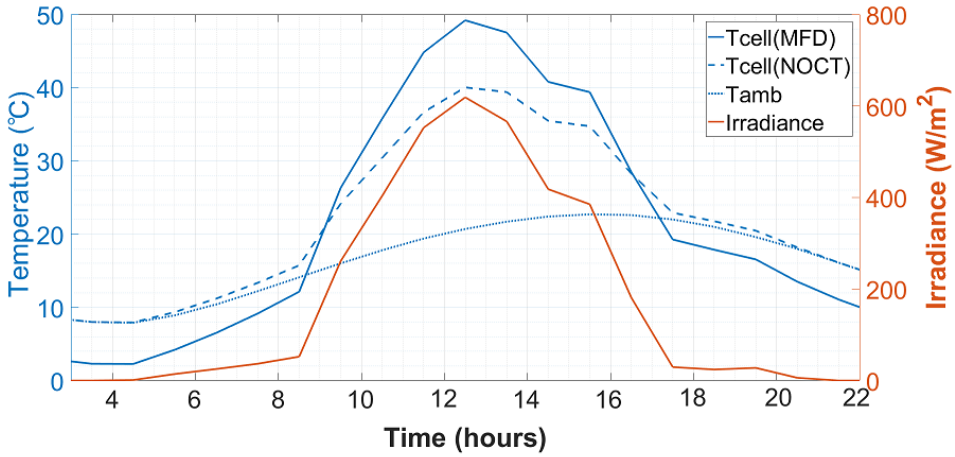

Figure 4.2: Simulated cell temperature using MFD and NOCT models for a sunny day.

is lower than T_{amb} (see equation 4.4) which results in the decrease of $T_{cell}(MFD)$. Therefore, the trend of lower $T_{cell}(MFD)$ as compared to T_{amb} can be attributed to varying values of T_{sky}.

4.4. Conclusions

The first goal of this chapter was to develop a thermal model that can predict the temperature of every solar cell in the PowerWindow for every hour of the year. The second goal was to compare the developed MFD to the conventional NOCT model. The thermal model developed for the case of the PowerWindow is more detailed as compared to the NOCT model to sufficiently estimate and justify the cell temperatures exposed to a particular kind of environment taking into account several factors. The cell temperatures from the MFD model as well as the incident irradiation obtained from the optical model will be used as inputs to the electrical model, which is explained in the next chapter.

5

Electrical Modelling

The computation of the incident irradiance on (Chapter 3) and temperatures (Chapter 4) of the solar cells inside the PowerWindow enable the determination of the DC power output and daily energy yield of the PowerWindow. In order to do so, this chapter aims to develop a detailed equivalent circuit model for each cell within the PowerWindow in order to simulate its electrical behaviour under non-uniform incident irradiance and cell temperatures. Moreover, it aims to discuss the effect of the following on the daily energy yield of the PowerWindow:

1. Different irradiation profiles such as a summer, winter and overcast day;
2. Orientation;
3. Blocking and bypass diodes.

5.1. Electrical Modelling Approach

The most common approaches for simulating the electrical behaviour of a PV module are the empirical and physical model. The former is unable to incorporate architectural parameters of the cells in a module and outputs only the final power of the module. The latter, on the other hand, is very flexible in that aspect and is able to produce not only the power output but also multi-level I-V curves [33]. A physical-based circuit modelling approach has been considered in this chapter as it is the most popular technique to model a solar cell. The advantages of this method include the effects of saturation current, resistances and more, that can be individually tuned to fit model requirements. There are many circuit simulation soft-wares like QUCS [22], LTspice [36], PCID [37] that have been used to simulate the electrical characteristics of a PV cell. In this study, the software QUCS is used as a result of its user-friendliness, cost-effectiveness and the ease of linking to MATLAB. Using this circuit modelling method and data processing through MATLAB as seen in Figure 5.1, it is possible to predict the daily energy yield of the PowerWindow as well as its DC power output.

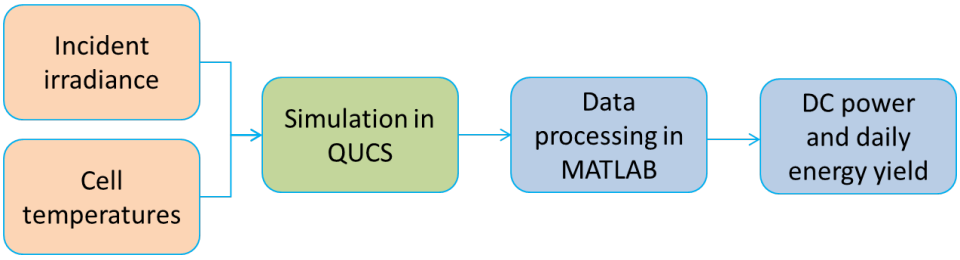

Figure 5.1: Electrical model flow chart displaying different steps required for the calculation of DC power and daily energy yield.

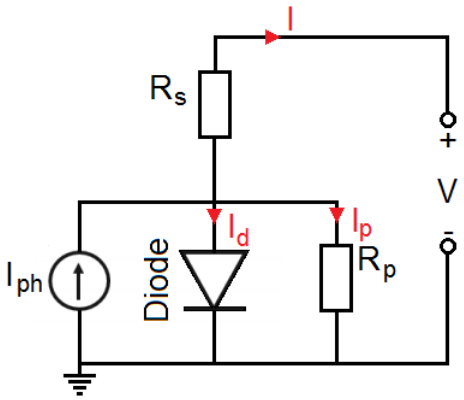

Figure 5.2: One Diode representation of a PV cell.

5.1.1. Electrical Circuit

While there are many ways to represent the equivalent circuit of a PV cell [38], one of the simplest representations is the one-diode model. It balances between accuracy and circuit complexities, which results in lower computation time.

Figure 5.2 is the one diode equivalent circuit of a PV cell. It takes into consideration the current source I_{ph}, the diode, and series and parallel resistances R_s and R_p of the solar respectively. For this circuit, the parameter sweep is across the DC voltage source rather than a load resistor in order to get an output. This output (current, voltage and power of the cell) is dependent not only on the sweep voltage range but also on the component values of this circuit. Different parameters like short-circuit current, open-circuit voltage, maximum power point, fill factor, etc. can be extracted from the data obtained after the I-V curve simulation in QUCS. The circuit modelling approach that is similar to [22, 39] is used in this research.

5.1.2. Electrical Parameters for Simulation

There are several equations that are needed to obtain the output electrical parameters pertaining to the circuit given in Figure 5.2. The total current I of this circuit can be found by Kirchhoff's current law and is displayed in equation 5.1.

$$I = I_{ph} - I_{sat}\left[\exp\left(\frac{V + I.R_s}{n.V_t}\right) - 1\right] - \left[\frac{V + I.R_s}{R_p}\right] \tag{5.1}$$

Where, I_{ph} is the photo-current, I_{sat} is the reverse bias saturation current of the diode, n is the ideality factor V_{th} is the thermal voltage given in the equation 5.2.

$$V_t = \frac{k.T}{q} \tag{5.2}$$

where, k is the Boltzmann constant, q is the electronic charge and T is temperature in Kelvin [4].

Photo-current

The current generated when light is incident on a PV cell is called photo-current. Often I_{ph} is considered to be equal to the short-circuit current (I_{sc}) of the PV cell. Since, it is dependent on both incident irradiance on and the operating temperature of PV cell, an approximation proposed by Luque-Sala and Duffie & Beckman can be used to obtain the expression for I_{ph} as seen in equation 5.3 [22].

$$I_{ph} = \frac{I_{SC,STC}.G.\left(1 + \alpha.\left(T_M - T_{M,STC}\right)\right)}{G_{STC}} \tag{5.3}$$

Where, G is the irradiance incident on the PV cell in W/m^2 obtained from optical modelling chapter, G_{STC} is the irradiance at standard test conditions (= 1000 W/m^2), T_M is the PV cell temperature obtained from the Chapter 4, $T_{M,STC}$ is the temperature of the cell at standard test conditions (= 25 °C) and α is the thermal coefficient of I_{sc} (= 2×10^{-5} A/°C) (refer Chapter 2).

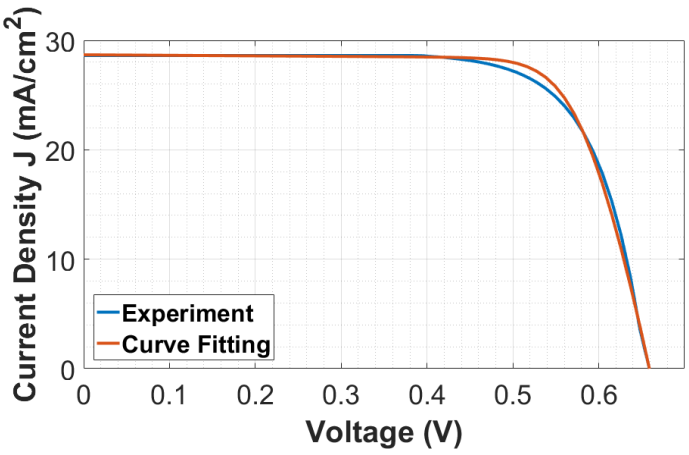

Figure 5.3: J-V curve obtained with curve-fitting using experimental values for a single cell.

Saturation Current

Empirical tests based on the approximation Duffie & Beckman were done to study the effects of operating temperature of a PV cell on I_{sat}. Equation 5.4 was obtained as a result of the study [22].

$$I_{sat} = \frac{I_{ph}}{\left(\exp \frac{q.(V_{OC,STC}+\beta.(T_M - T_{M,STC}))}{n.k.T_{M,STC}} - 1\right)} \tag{5.4}$$

Where, $V_{oc,STC}$ is the open circuit voltage of the PV cell, and β is the thermal coefficient of V_{oc} (= -1.6 × 10^{-3} V/°C) (refer Chapter 2).

It can be seen from section 5.1.2 and 5.1.2 that the both incident irradiance on and the temperature of the PV cells have been incorporated as an input into the final electrical model.

Series and Shunt Resistances

The series (R_s) and shunt (R_p) values were determined using a technique called *curve-fitting*. In this technique, an experimental J-V curve is used as a reference and R_s and R_p are found through an iterative method performed in MATLAB using equation 5.1 after deleting the I_{ph} term. The values of R_s and R_p are tuned to fit the experimental values. The R_s and R_p are determined by the slope of curve at V_{oc} and J_{sc} points respectively. It can be seen in Figure 5.3 that the accuracy of the fit is high near the short-circuit and open-circuit points. Therefore, the values obtained for the resistances are very close to accurate. The total fit of the curve (R^2 value) was found to be ≈ 0.97.

Ideality Factor

The ideality factor used for the simulations was determined by the dark current measurements reported in Chapter 2. An ideality factor of 1.28 was used.

Comparison to Experimental Values

The experimental data of the mini-module was compared to that simulated in QUCS at STC conditions. It is observed in Figure 5.4 that both curve profiles are very similar barring the differences in the Fill Factor (*FF*) and the maximum power point (P_{mpp}) The percentage difference between the *FF* and P_{mpp} was found to be 2 % and 4 % respectively, which are acceptable values.

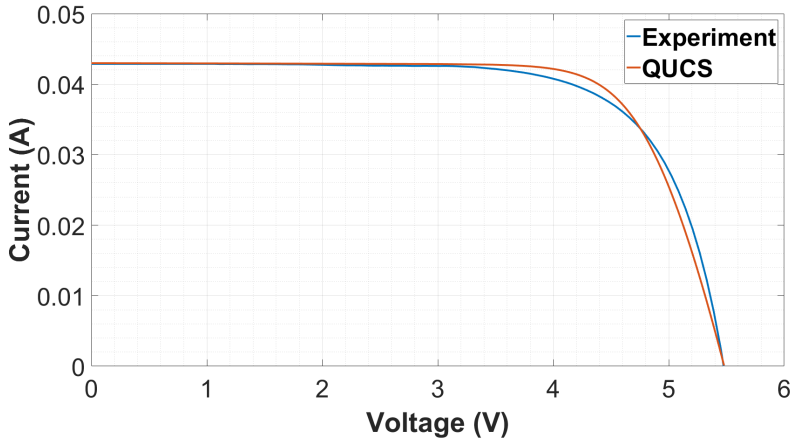

Figure 5.4: Experimental and simulated I-V curve for a mini-module at STC.

5.1.3. Modelling Circuit Configurations

Bypass Diode

The working principle of a bypass diode is to counter-act the effects of shading on solar modules by providing a low resistance path for the current when these modules are connected in series. It is connected parallel to but in reverse with solar modules. When the PV module is illuminated, the module conducts while when it is shaded, the bypass diode conducts [4].

In order to understand the effect of bypass diodes on the daily energy yield of the PowerWindow, it is necessary to evaluate different configurations of the equivalent circuit involving the bypass diode. Each PowerWindow consists of 3 PowerBars that are connected in parallel, each with their own maximum power point tracker (MPPT). Therefore, the circuit of the PowerWindow could be reduced to a PowerBar and three separate simulations for each PowerBar were conducted in order to perform the simulations at a faster rate.

The equivalent circuit of a PowerBar is shown in Figure 5.5 (a) where the blue rectangle represent the mini-modules (refer to Figure 1.3). Three mini-modules are connected in series, each with its own bypass diode (green). A PowerModule is constructed by connecting one blocking diode (orange) in series with the series connected mini-modules. Four such PowerModules are connected in parallel to make one PowerBar. Four different equivalent circuit configurations of a PowerBar seen in Figure 5.5, without changing the voltage of the system, are studied in this chapter to determine which equivalent circuit results in the maximum energy yield. Figure 5.5 (a) is the schematic that is currently being used by Physee. Figure 5.5 (b) is the schematic created to understand the effect of self-shading and inhomogeneous irradiation without using any bypass diodes.

Blocking Diode

Blocking diodes facilitate the flow of current in only one direction by not allowing the current to flow in the reverse direction. Its working principle is to reduce the losses pertaining to mismatch between PV arrays connected in parallel by blocking current flow into arrays that produce less current as compared to their counterparts. Consequently, this allows the isolation of strings that are shaded from the rest of the system [4]. Figure 5.5 (c) describes the case that was studied to understand the effects of blocking diodes on the energy yield of the PowerWindow.

Moreover, the effect of having no diodes (Figure 5.5 (d)) in the PV system is also evaluated on the basis of daily energy yield.

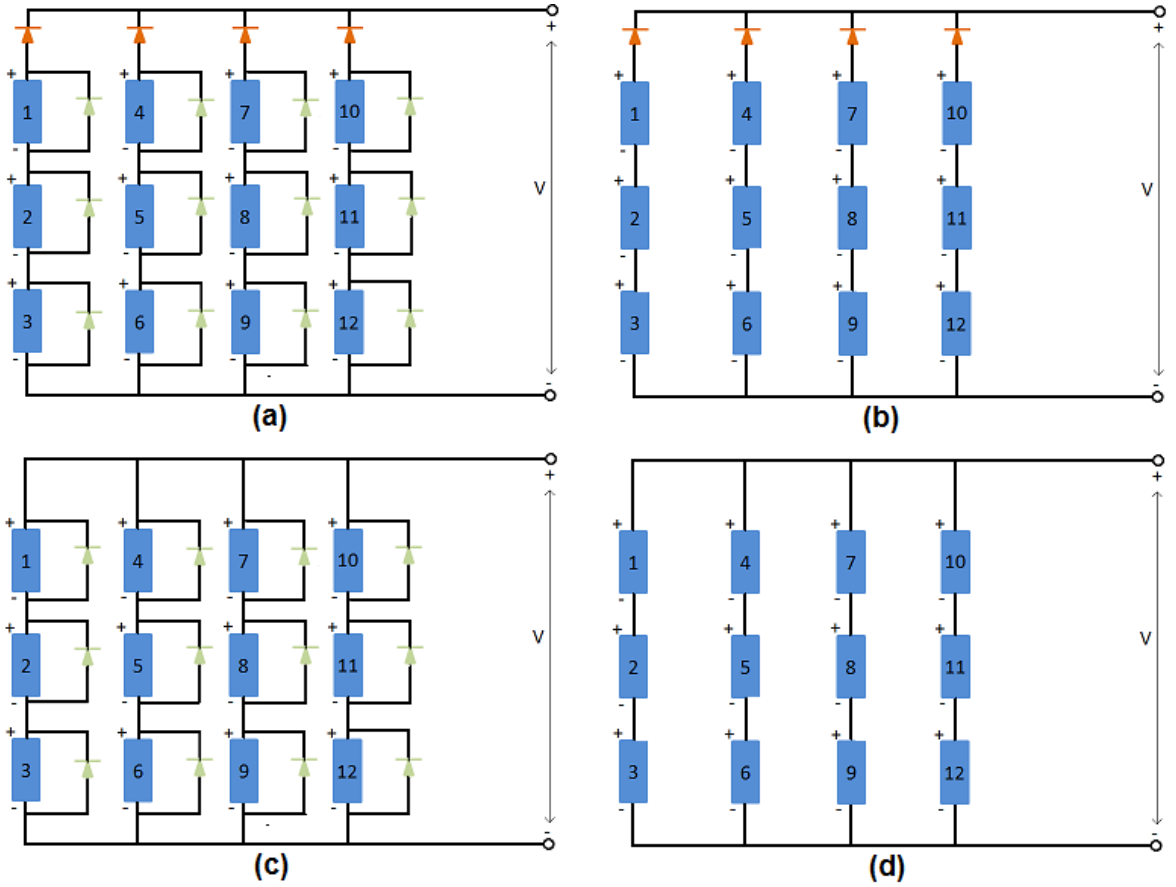

Figure 5.5: Different equivalent circuit configurations using (a) 12, (b) 0 number of bypass diodes, (c) 0 and (d) number of blocking diodes for a PowerBar.

5.1.4. Analysis

The results from all the simulations are analysed on the basis of DC power output ($P_{mpp,DC}$) and daily energy yield ($E_{DC,day}$) calculations of a PowerWindow. The daily energy yield can be done by integrating the maximum DC power output ($P_{mpp,DC}$) over a given time period (t). In this case, t is one day. The formula for the calculation of daily energy yield in given in equation 5.5 [4].

$$E_{DC}^{day} = \int_{day} P_{mpp,DC}(t)\, dt \tag{5.5}$$

5.2. Results

5.2.1. Effect of Different Irradiation Conditions

The PowerWindow can have a varied DC power output depending on the irradiation that is incident on and the temperature of the solar cells inside it. Studying the effect of different irradiation conditions can facilitate the understanding of the DC power output profile of the PowerWindow in those conditions. As mentioned in Section 5.1.3, the electrical circuit for the PowerBar was used since each PowerBar has its own Maximum Power Point Tracker. Therefore, the energy generated from year PowerBar could be cumulatively added to determine the total DC energy yield of the PowerWindow.

Figure 5.6 displays the DC power output of as well as the average incident irradiation on the three PowerBars in a PowerWindow facing south for a summer, winter and overcast day in Eindhoven. It can be seen that on all the three days, the DC power output profile follows the irradiation profile incident on the cells.

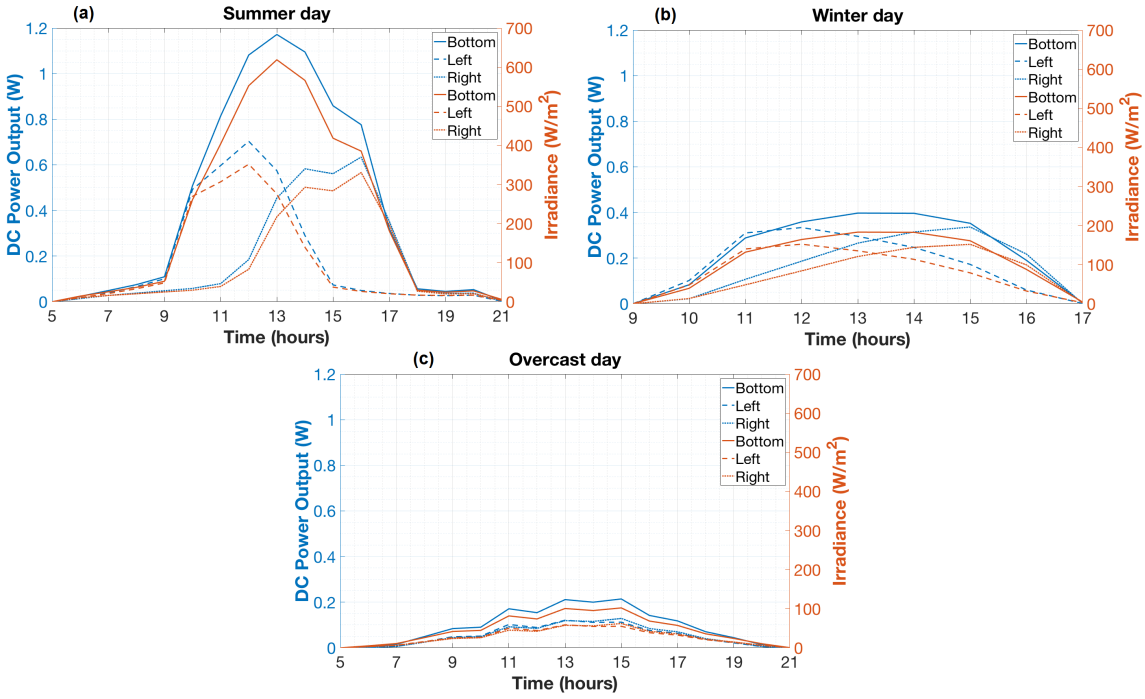

Figure 5.6: DC power output of the bottom, left and right PowerBar with respect to average incident irradiation on each PowerBar on a (a) summer, (b) winter and (c) overcast day for a south facing PowerWindow.

For a summer day (Figure 5.6 (a)), the power produced by the bottom PowerBar peaks at 1 pm. The left PowerBar produces power in the first half of the day, peaking at solar noon owing to its orientation towards south-east. The right PowerBar generates power from noon to evening as a result of being oriented towards south-west. Moreover, the bottom PowerBar produces almost double the power produced by left or right PowerBars. This is because the bottom PowerBar is oriented towards the south and is sensitive to south-east, south and south-west orientations, and produces a power output throughout the day unlike its counter-parts. The maximum power produced by the bottom PowerBar is $\approx$ 1.2 W.

A similar DC power output profile is seen in the case of a winter day (Figure 5.6 (b)). However, the average irradiation received on the solar cells is less than 250 W/m^2 and consequently, the maximum DC power output from one PowerBar is limited to 0.4 W. Although the bottom PowerBar has a larger DC power output than the left and right PowerBar, it does not produce double the power as compared to its counter-parts.

For an overcast day (Figure 5.6 (c)), the left and right PowerBars generate almost the same amount of DC power while the bottom PowerBar produces double the power output of either left or right PowerBar. Since the irradiation received by the cells is $\approx$ 100 W/m^2, the maximum DC power output is only 0.2 W.

The daily energy yield of each PowerBar in a PowerWindow is obtained by integrating the area under the DC power output versus time curve. This daily energy yield is displayed for the summer, winter and overcast days in Figure 5.7. For a typical overcast, summer and winter day, a total of $\approx$ 3 Wh, 13 Wh and 5 Wh of energy is produced respectively. On all the three days, the bottom PowerBar produces the highest amount of energy. It constitutes of half the energy produced on a typical summer and overcast day.

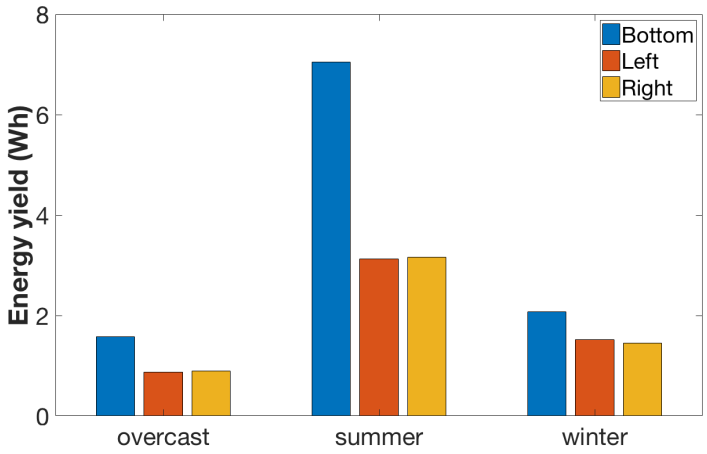

Figure 5.7: Daily energy yield of the bottom, left and right PowerBar for a summer, winter and overcast day for a south facing PowerWindow.

5.2.2. Effect of Orientation of the PowerWindow

This section analyses the performance in terms of both DC power and energy output of a PowerWindow when it is oriented in different directions in one geographical location. This study is conducted for a typical summer, winter and overcast day in Eindhoven.

Figure 5.8 displays the DC power output versus the time of a PowerWindow when it is oriented to the north, east, west and south for the city of Eindhoven.

For a summer day (Figure 5.8 (a)), peak production of the PowerWindow facing south is reached at solar noon. The east and west facing PowerWindows produce the maximum power in the morning and evening respectively as a result of their orientation towards the sun at those times. Additional, it can be seen that they are almost symmetrically opposite to one another in terms their power production profiles. The north facing PowerWindow, two small bumps are observed in the morning and evening as a result of direct irradiation present in the north-east and north-west on this day. The PowerWindow produces < 3 W of peak power regardless of orientation.

On a winter day (Figure 5.8 (b)), a similar trend with DC power production profile of the east and west facing PowerWindows is seen. However, on this day, their peak production is less that than of a south facing PowerWindow. Although the south facing PowerWindow produces the highest amount of power, the maximum power produced by it is ≈ 1 W only. As a consequence of the sun position in the winter months, the north facing PowerWindow does not receive any direct sunlight and therefore, is limited to a peak power of < 0.25 W due to diffused irradiation.

For an overcast day, all PowerWindows in the four orientations produce the same amount of power and it is difficult to distinguish their power output individually (Figure 5.8 (c)). This is due to the fact that only diffused irradiation is present in the sky on this day. There is no clear distinction in the production profile of especially the north and the south facing PowerWindows since they all produce less than 0.5 W.

The DC energy yield of the PowerWindows oriented in all the four directions for summer, winter and overcast days is given in Figure 5.9. The maximum energy produced for an overcast, summer and winter day are ≈ 3 Wh, 5Wh and 16 Wh respectively. The west and east facing PowerWindow produce the most energy in the summer since there is higher irradiation present from the morning to evening and they are oriented towards the sun position (refer to Section 3.2.3). The south facing PowerWindow produces the highest amount of energy on the winter day since sunlight is available starting from 9 am unlike 5 am on a summer day.

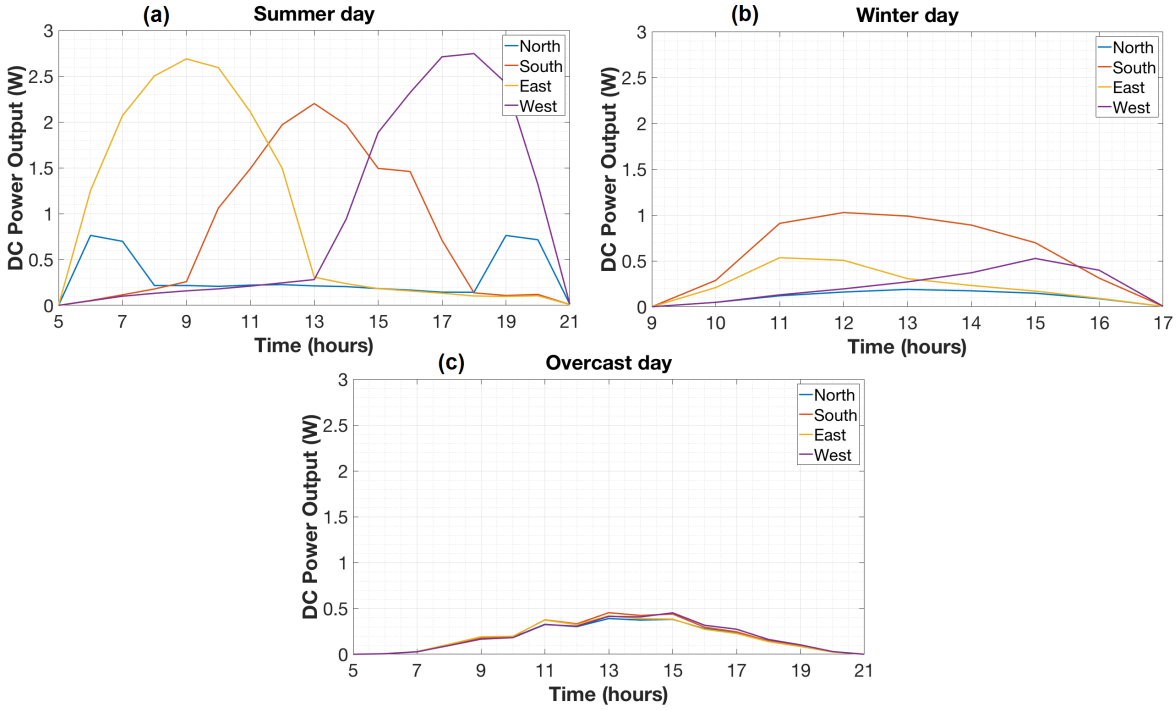

Figure 5.8: DC power output of a PowerWindow on a (a) summer day, (b) winter day and (c) an overcast day in Eindhoven.

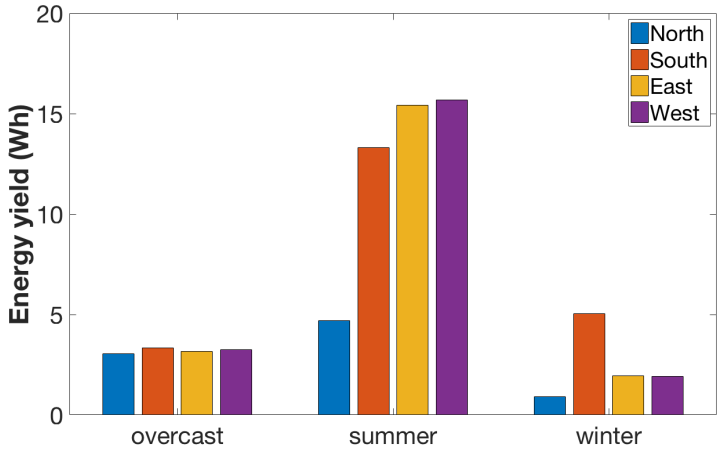

Figure 5.9: Daily energy yield of a PowerWindow when placed in on summer, winter and overcast day in Eindhoven .

5.2.3. Effect of Blocking and Bypass Diodes

The effect of different configurations, as described in Section 5.1.3, is evaluated in this section. In order to understand how these configurations affect the energy yield of a PowerWindow, it is crucial to analyze the I-V curves of a uniformly illuminated PowerBar. This graph is given in Figure 5.10. It is evident from this graph that the I-V curves of Figures 5.5 (a) and (b), represented in blue and red lines, are the same. This is because the bypass diodes are not active when all the cells receive the same irradiation. The current from each PowerModule flows through the blocking diode and therefore, a tail is observed at the V_{oc} of both these curves. This tail is a combination of the forward characteristics of the blocking diode and the I-V curve if the PowerBar. Additionally, the I-V curves of Figures 5.5 (c) and (d), represented in yellow and purple lines, are the same. Since these configurations have no blocking diodes, there is no tail observed at the V_{oc}. However, there is a slight increase in the V_{oc} as compared to the other two cases. The percentage difference of the P_{mpp} between

Figures 5.5 (a) and (b), and Figures 5.5 (c) and (d) is 6%.

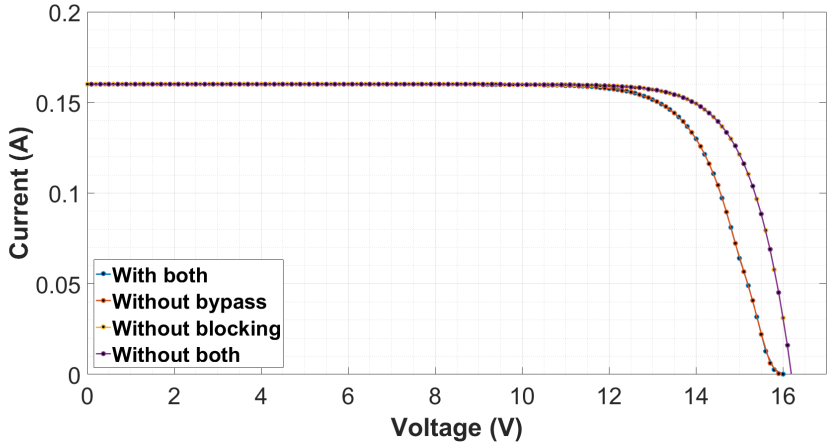

Figure 5.10: I-V curve of a PowerBar illuminated uniformly at 1000W/m^2 different diode configurations.

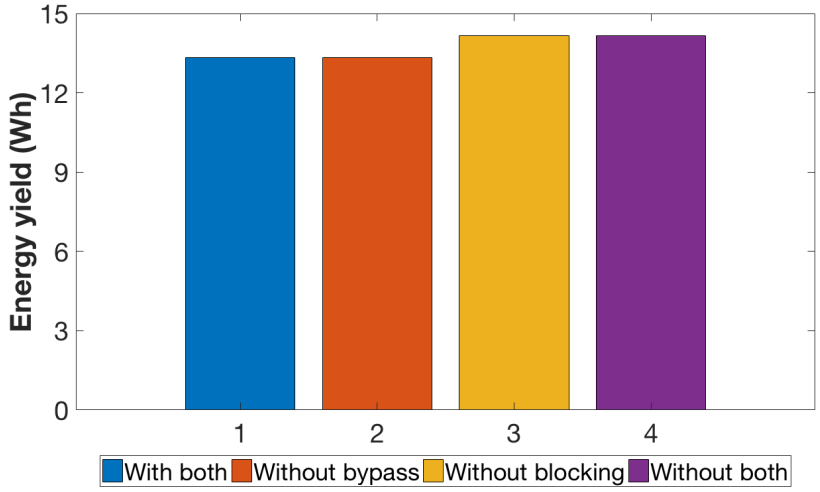

Figure 5.11: Energy yield of a PowerWindow with different diode configurations for a summer day in Eindhoven .

The energy yield of a PowerWindow with the diode configurations for a PowerBar shown Figure 5.5 is displayed in Figure 5.11. The energy yield data is in accordance with the result obtained with the I-V curves in Figure 5.10. Even here, there is a decrease of ≈ 6 % in the energy yield of a PowerWindow in the configurations displayed in Figure 5.5 (a) and (b) with respect to the configurations displayed in Figure 5.5 (c) and (d). Although bypass diodes do not improve the performance of the PowerWindow, they protect the PowerWindow against different shading conditions the PowerWindow can be exposed to. However, the blocking diodes reduce the energy yield of the PowerWindow by ≈ 6 % as a result of their forward drop voltage. The best performance in terms of energy can be seen when the PowerWindow has no diodes or has only bypass diodes. Despite having no diodes, configuration (d) in Figure 5.5 is not the best since it does not protect the PW when it is exposed to different shading conditions . The same argument holds true for the bypass only (without blocking) configuration. Thus, the configuration that is performance effective and protects the PW against different shading conditions seems to be the one with both diodes.

5.3. Conclusions

The goal of this chapter was to evaluate the effect of different irradiation conditions on, orientation and bypass and blocking diodes configurations of the PowerWindow on its daily energy yield. Section 5.2.1 explains the effect of a summer, winter and overcast day on a south facing PowerWindow in Eindhoven. It was found that maximum energy the PowerWindow can produce on a typical summer, winter and overcast day was 13 Wh, 5 Wh and 3 Wh. Furthermore, it was concluded that the bottom PowerBar produces almost double the energy as compared to the left and right PowerBar on those three days. Section 5.2.2 describes the effect of the orientation of the PowerWindow when it faces in north, south, east and west on a summer, winter and overcast day in Eindhoven. It was found the energy yield of differently oriented windows was the same for an overcast day while, it was very different for a summer and winter day. The effect of blocking and bypass diodes was explained in Section 5.2.3. It was concluded that the most performance effective configuration that also protects the PW when it may be exposed to different shading conditions is the one with both bypass and blocking diodes. More research needs to be done in order to correctly estimate the number of bypass diodes using different shading conditions through optical and electrical simulations, and experiments.

6

Conclusions and Recommendations

6.1. Conclusions

The goal of this thesis was to model the energy yield of the PowerWindow. This was done by developing a simple framework involving optical, thermal and electrical models.

It was found that the DC power output is heavily dependent on the type of glass used since this changed the irradiance incident on the solar cells. It is ideal to use clear glass instead of stripped glass in order to have a 10 % higher DC power output per PowerModule. Therefore, the anti-NIR coating must not be stripped away mechanically but instead be cut to a size that does not cover the solar cells under all possible sun paths before being applied to the PowerWindow. The maximum power that a stripped PowerWindow can produce under a solar simulator was found to be $\approx$ 3.5 W.

The PowerWindow consists of three PowerBars that are oriented in different directions, with a tilt of 90° (left and right PowerBar) and 45°. This resulted in each them having a different time of day in which they produced power. Self-shading of the PowerWindow was evaluated in terms of the irradiance incident on the solar cells. It was concluded that the effect of self-shading is only visible in the summer months and affected only 3 cells for a south facing PowerWindow.

The results from the electrical modelling suggested that the configuration involving both the bypass and blocking diodes was the best in terms of performance and protecting the solar cells. A loss of 6 % in DC power output and energy yield was seen as a result of using blocking diodes. However, it was concluded that more simulations and experiments are needed in order to estimate the correct number of bypass diodes using different shading conditions.

The results of the DC energy yield simulation for a summer, winter and overcast day in Eindhoven was 13, 5 and 3 Wh using the configuration with both the blocking and bypass diodes. It was also found that a west and east facing PowerWindow generated more energy than a south facing PowerWindow. However, the south facing PowerWindow produced the most power in the winter. On an overcast day, the PowerWindow produced 3 Wh regardless of its orientation.

6.2. Recommendations

The focus of this thesis is on the performance analysis of the PowerWindow in terms of its daily energy yield. Further research can be done in the application of PowerWindow from a photovoltaic system stand point. It will be interesting to study the yearly energy yield of a building made of PowerWindows in different geographical locations.

Shading analysis of structures close to the vicinity of the PowerWindow can be taken into consideration in the optical model. Additionally, this model can be coupled with LIDAR data implemented with Sketchup or similar tools to include the effect of objects that are far off on the horizon of the PowerWindow.

This thesis employs a relatively simple steady state thermal model to predict the temperature of the solar cells. A new transient temperature model for the entire PowerWindow, including the glasses, can be developed using the approach of thermal energy balances via the fluid dynamic method. This study can then predict the temperatures of every component within the PowerWindow and facilitate in making a new design of the PowerWindow that leads to a better performing system in terms of energy yield. It can be combined with the durability and reliability studies to evaluate the robustness of the PowerWindow. Experiments like accelerated lifetime testing can be performed and analysed. Futhermore, the effect of geography in terms of the temperature and final energy yield of the PowerWindow can also be researched.

This thesis provides a solid foundation for further electrical design optimisation for the PowerWindow. Shading analysis coupled with optical modelling, opto-electronic tests and the electrical model developed on QUCS can help in finding the circuit architecture suitable for best performance of the PowerWindow. This includes the effect of self-shading and other external shading conditions that the PowerWindow may be exposed to. Lastly, feasibility studies of a large-scale PowerWindow project can be done the basis of Levelized Cost Of Electricity and the Return Of Investment.

Bibliography

[1] United Nations, "Towards a Green Economy: Pathways to Sustainable Development and Poverty Eradication", UNEP, 2011. Available at: *www.unep.org/greeneconomy*

[2] Y. Zhongguo ke xue, "Power of Renewables: Opportunities and Challenges for China and the United States", National Academies Press, Chapter 4, 2010.

[3] D. MacKay, "Sustainable Energy - Without The Hot Air", 1st ed. Cambridge: UIT Cambridge, 2013.

[4] A. Smets, K. Jager, M. Zeman, O. Isabella, R. v. Swaaij, "Solar Energy: Fundamentals, Technology and Systems", UIT Cambridge Ltd., v.1., 2016.

[5] European Commission, "Buildings - Energy - European Commission", Energy, 2017. Available: *https://ec.europa.eu/energy/en/topics/energy-efficiency/buildings*

[6] United Nations Environment Programme (UNEP), "Why Buildings", 2017. Available: *http://staging.unep.org/sbci/AboutSBCI/Background.asp*

[7] European Commission,"Nearly zero-energy buildings - Energy - European Commission", Energy, 2017. Available: *https://ec.europa.eu/energy/en/topics/energy-efficiency/buildings/nearly-zero-energy-buildings*

[8] IXYS,"IXYS Website > Product Portfolio > Green Energy", Ixys.com, 2018. Available: *https://www.ixys.com/ProductPortfolio/GreenEnergy.aspx*

[9] M. A.Green, "Solar cell efficiency tables (version 49)", Progress in Photovoltaics: Research and Applications, vol 25, Issue 4, pp. 333–334, 2017.

[10] PVsyst Photovoltaic software,"Home", Pvsyst.com, 2018. Available: *http://www.pvsyst.com/*

[11] National Renewable Energy Laboratory, "System Advisor Model (SAM)", sam.nrel.gov, 2018. Available: *https://sam.nrel.gov/*

[12] D. T. Reindl, W. A. Beckman, and J. A. Duffie, "Evaluation of hourly tilted surface radiation models", Solar Energy 45, 9, 1990.

[13] Perez, R. Seals, R. Stewartt, and D. Menicucci, "A new simplified version of the Perez diffuse irradiance model for tilted surfaces", Solar Energy 39, 221, 1987.

[14] M. Lave, W. Hayes, A. Pohl, and C. W. Hansen, "Evaluation of global horizontal irradiance to plane-of-array irradiance models at locations across the United States", IEEE Journal of Photo-voltaics 5, 597, 2015.

[15] R. Santbergen, V. Muthukumar, R. Valckenborg, W. van de Wall, A. Smets and M. Zeman, "Calculation of irradiance distribution on PV modules by combining sky and sensitivity maps", Solar Energy, vol. 150, pp. 49-54, 2017.

[16] R. Perez, R. Seals and J. Michalsky, "Modeling Skylight Angular Luminance Distribution from Routine Irradiance Measurements", Journal of the Illuminating Engineering Society, vol. 22, no. 1, pp. 10-17, 1993.

[17] S. Vergura, G. Acciani and O. Falcone, "3-D PV-cell model by means of FEM", International Conference on Clean Electrical Power: Renewable Energy Source Impact, vol. 2, pp. 35-40, 2009.

[18] M. K. Fuentes, "A Simplified Thermal Model for Flat-Plate Photovoltaic Arrays", Sandia Report, 1987.

[19] M. G. Villalva, J. R. Gazoli, and E. R. Filho, “Comprehensive Approach to Modeling and Simulation of Photovoltaic Arrays”, IEEE Transaction on Power Electronics, vol. 24, pp. 1198-1208, 2008.

[20] D. Sera, R. Teodorescu and P. Rodriguez, “PV panel model based on datasheet values”, in IEEE International Symposium on Industrial Electronics, Jun., pp. 2392- 2396, 2007.

[21] A. Durgadevi, S. Arulselvi and S. P. Natarajan, “Photovoltaic modeling and its characteristics”, International Emerging Trends in Electrical and Computer Technology Conference, pp. 469- 475, 2011.

[22] M. Pareja, J. Pelegri-Sebastia, T. Sogorb and V. Llario, "Modeling of Photovoltaic Cell Using Free Software Application for Training and Design Circuit in Photovoltaic Solar Energy", New Developments in Renewable Energy, 2013.

[23] Keithley, "Making I-V and C-V Measurements on Solar/Photovoltaic Cells Using the Model 4200-SCS Semiconductor Characterization System", Application Note Series, Number 2876, Keithley, U.S.A, 2007.

[24] ASTM Compass, "ASTM E927 Standard Specification for Solar Simulation for Terrestrial Photovoltaic Testing", 2015.

[25] A. Zekry and A. Al-Mazroo, "A distributed SPICE-model of a solar cell", IEEE Transactions on Electron Devices, vol. 43, no. 5, pp. 691-700, 1996.

[26] IXYS, "IXOLARTM High Efficiency SolarBIT", Ixapps.ixys.com, 2018. Available: *http://ixapps.ixys.com/datasheet/kxob22-12x1l-data-sheet-20130902-.pdf*

[27] IXYS, "IXOLARTM High Efficiency SolarMD", Ixapps.ixys.com, 2018. Available: *http://ixapps.ixys.com/DataSheet/20110107-SLMD121H08-DATA-SHEET.pdf*

[28] S. Regondi, "Solar-Powered Infotainment Spot 2.0: Design and fabrication of a prototype in collaboration with Kaneka Corporation", Master Thesis, Delft University of Technology, June, 2017. Available at: *uuid:8abce479-87d4-49bb-8056-cc11f5345206*

[29] "Meteonorm: Irradiation data forevery place on Earth", Meteonorm.com, 2018. [Online]. Available: http://www.meteonorm.com/

[30] M. Rubin, *Calculating heat transfer through windows*, International Journal of Energy Research, vol. 6, no. 4, pp. 341-349, 1982.

[31] J. A. Duffie, W. A. Beckman, W. M. Worek, Journal of Solar Energy Engineering, Vol. 116, p. 67, 2003.

[32] E. Skoplaki, J. A. Palyvos, "Operating temperature of photovoltaic modules: A survey of per-tinent correlations", Renewable Energy 34, p. 23, 2009.

[33] G. J. Faturrochman, "Design Optimization of Bifacial Photovoltaic Noise Barriers Using a High Granularity Energy Yield Modelling Approach", Master Thesis, Delft University of Technology, June, 2017. Available at: *uuid:27d291f3-5ec7-4cc1-8c78-5277180003bf*

[34] H. Zondag, D. de Vries, W. van Helden, R. van Zolingen and A. van Steenhoven, "The thermal and electrical yield of a PV-thermal collector", Solar Energy, vol. 72, no. 2, pp. 113-128, 2002.

[35] J. Graebner and K. Azar, "Thermal Conductivity Measurements in Printed Wiring Boards", Journal of Heat Transfer, vol. 119, no. 3, p. 401, 1997.

[36] S. Guo, F. Ma, B. Hoex, A. Aberle and M. Peters, "Analysing Solar Cells by Circuit Modelling", Energy Procedia, vol. 25, pp. 28-33, 2012.

[37] V. d’Alessandro, F. Di Napoli, P. Guerriero and S. Daliento, "An automated high-granularity tool for a fast evaluation of the yield of PV plants accounting for shading effects", Renewable Energy, vol. 83, pp. 294-304, 2015.

[38] A. Jordehi, "Parameter estimation of solar photovoltaic (PV) cells: A review", Renewable and Sustainable Energy Reviews, vol. 61, pp. 354-371, 2016.

[39] Vimal Adithyan Muthukumar, "Irradiance and energy yield modelling of fexible thin module", SIP-2 project, PVMD, TU Delft, 2017.